Islamic University of Technology

Department of Mechanical and Production Engineering

Thermodynamic Investigation of Combined Cycles And Polygeneration Systems With An Emphasis On Supercritical Carbon Dioxide Power Cycles

A Thesis by

SALIM SADMAN BISHAL
DEWAN FAHIM FAYSAL

Submitted in Partial Fulfillment
of the Requirements
for the Degree of

Bachelor of Science in Mechanical Engineering

May 2022

Thermodynamic Investigation of Combined Cycles And Polygeneration Systems With An Emphasis On Supercritical Carbon Dioxide Power Cycles

SALIM SADMAN BISHAL, 170011014

DEWAN FAHIM FAYSAL, 170011036

Session: 2020-2021

Submitted in Partial Fulfillment
of the Requirements
for the Degree of

Bachelor of Science in Mechanical Engineering

DEPARTMENT OF MECHANICAL AND PRODUCTION ENGINEERING

May 2022

CERTIFICATE OF RESEARCH

This thesis titled "Thermodynamic Investigation of Combined Cycles And Polygeneration Systems With An Emphasis On Supercritical Carbon Dioxide Power Cycles" submitted by SALIM SADMAN BISHAL (170011014) and DEWAN FAHIM FAYSAL (170011036) has been accepted as satisfactory in partial fulfillment of the requirement for the Degree of Bachelor of Science in Mechanical Engineering.

Supervisor

_____

Dr. Mohammad Monjurul Ehsan
Associate Professor
Department of Mechanical and Production Engineering (MPE)
Islamic University of Technology (IUT)

Head of the Department

_____

Dr. Md. Anayet Ullah Patwari
Professor
Department of Mechanical and Production Engineering (MPE)
Islamic University of Technology (IUT)

DECLARATION

We hereby declare that this thesis entitled "Thermodynamic Investigation of Combined Cycles And Polygeneration Systems With An Emphasis On Supercritical Carbon Dioxide Power Cycles" is an authentic report of our study carried out as requirement for the award of degree B.Sc. (Mechanical Engineering) at Islamic University of Technology, Gazipur, Dhaka, under the supervision of Dr. Mohammad Monjurul Ehsan, Associate Professor, MPE, IUT in the year 2022

The matter embodied in this thesis has not been submitted in part or full to any other institute for award of any degree.

_____

Salim Sadman Bishal
170011014

_____

Dewan Fahim Faysal
170011036

ACKNOWLEDGMENTS

First of all, we would want to express our gratitude to our Almighty Allah for providing us with the power, knowledge, skill, and chance to conduct this research and make it a success.

We would like to express our huge gratitude to our supervisor, of Dr. Mohammad Monjurul Ehsan, Associate Professor, MPE, IUT, who gave us access to the vast world of science and led us through it with his wise ideas, huge patience, and constant encouragement. during the realization of this project. We couldn't have asked for a better guide and teacher for this study.

We thankfully acknowledge the support and inspiration that we received from my teachers especially Mr. Sayedus Salehin and Mr. Mohammad Raihan Uddin at very beginning of the project. We are also thankful to the MPE department of the Islamic University of Technology for being helpful, giving us a lot of personal and professional assistance, and teaching us a great deal in becoming mechanical engineer.

Additionally, we would like to thank to our beloved friends who supported and motivated us and stood beside us throughout our academics.

Finally, we would like to express our huge thanks to our respected parents and family members for their endless love, and emotional, financial and moral support in completing our bachelor’s degree. We dedicate our thesis to our respective families.

ABSTRACT

Because of the tremendous growth in global population and economic activity, as well as growing environmental concerns, efficient energy use will be critical in creating the future energy landscape. Reduced waste heat generation is an important step toward future waste heat usage success. The purpose was to investigate numerous thermodynamic systems and model a new one that uses sCO2 cycles, as well as other possible combinations, to successfully and efficiently recover waste heat for electricity production, cooling effect or heating. An integrated CCHP (cooling, heating, and power) strategy is developed recognizing the energy cascade efficiency for low/medium-grade heat waste, which merges multiple cycles, a sCO2 cycle and an Organic Rankine cycle (ORC) and an Absorption refrigeration cycle (ARC), and the topping cycle of a gas turbine cycle. Under working conditions, the energy utilization factor increases by 4.5 percent, according to the data. Using parametric analysis, the impact of design elements on the main performance parameters of the suggested system is studied. The consequences of the system's main parameters were graphically depicted. The goal is to research several systems and construct a modern one that uses sCO2 cycles, as well as other conceivable combinations, to effectively and reliably recover waste heat.

TABLE OF CONTENTS

LIST OF FIGURES

LIST OF TABLES

NOMENCLATURE

Symbols	Meaning
C_p	Specific heat at constant pressure
h	Specific enthalpy
$\dot{m}$	Mass flow rate
P	Pressure
T	Temperature
W	Power
r_p	Pressure ratio for gas turbine
s	Entropy
X	Recompressed mass flow ratio
x	Ammonia concentration
Q	Heat transfer rate
υ	Specific volume

GREEK LETTERS

Symbols	Meaning
γ	Specific heat ratio
η	Gas-turbine isentropic efficiency
ε	Effectiveness of heat exchangers

ABBREVIATIONS

Symbols	Meaning
LHV	Lower Heating Value
CC	Combustion Chamber
HE	Heat exchanger
HTR	Recuperator having High Temperature
LTR	Recuperator having Low Temperature
HPT	High pressure turbine
LPT	Low pressure turbine
AC	Air compressor
MC	Main Compressor
RC	Recompression Compressor
ARC	Absorption Refrigeration Cycle

SHE	Solution Heat Exchanger
PR	Pressure Ratio (recompression sCO2 cycle)
CIT	Compressor Inlet Temperature
EUF	Energy Utilization Factor
COP	Co-efficient Of Performance

SUBSCRIPTS

Symbols	Meaning
0	Reference environment
AC	Air compressor
GT	Gas turbine
cond	Condenser
abs	Absorber
eva	Evaporator
T	Turbine
gen	Generator
isen	Isentropic
in	Inlet
out	Outlet
c	Compressor

t	Turbine
high	Maximum condition
low	Minimum condition

Chapter 1
INTRODUCTION

1.1 Motivation

Because of massive expansion in the global population and economic activity, as well as growing environmental concerns, efficient energy utilization will be playing an important part in the formation of the energy landscape of the future. Conventional power plants, which rely on a single prime mover, are inefficient (39%) and waste a significant amount of energy. [1] These single prime mover powerplants generate a huge amount of low to mid-level waste heat daily from industrial activities that are not fully used. Low energy conversion efficiency makes them unsuitable for power generation. Reduced waste heat generation is a critical step toward successful usage of waste heat in future. Utilizing waste heat can be helpful to reach the highest level of thermal efficiency for any thermodynamic system. In the past, much attention and effort were executed toward the simplicity and reduction of cost of core power, cooling or heating generation systems. Building combined cycle plants or developing a polygeneration system to recover waste heat is an efficient approach to accomplish this. In combined cycle systems, waste heat from one cycle is used to power another cycle of an operation, whereas polygeneration systems have many outputs from a system besides power output, such as heating, cooling and freshwater production. Here waste heat generated from a standalone unit is employed to produce these outputs. Utilization of waste heat from a standalone thermodynamic cycle to produce freshwater, cooling and heat effect is an effective approach to utilize waste heat and maximize energy usage.

In addition to this, the supercritical CO2 (s-CO2) power cycle has attracted a growing amount of interest for a variety of applications over the course of the past twenty years due to the potential benefits it possesses over

traditional power generation methods. High thermal efficiency, compact turbomachinery, straightforward structure, and a smaller overall plant size are the primary advantages offered by the s-CO2 Brayton cycle. For mild intake turbine temperatures ranging from 500 to 800 degrees Celsius, this cycle can be viewed as an alternative to the steam Rankine cycle. Therefore, its applications span a broad spectrum, including the nuclear and fossil fuels, as well as waste heat recovery and utilizing renewable energy (solar, geothermal and fuel cells). This is the reason why the supercritical carbon dioxide Brayton cycle was the primary focus of this study. The goal to investigate various systems and develop a new one that utilizes sCO2 cycles along with other possible combination to recover waste heat successfully and efficiently.

1.2 Research Problem Statement

Using waste heat emitted from a standalone power producing cycle to reduce energy consumption or boost energy utilization factor by constructing multiple output, i.e., process heat, cooling effect, freshwater production systems while combining existing cycles.

1.3 Thesis Goals and Objectives

The goal was to research several thermodynamic systems and model a new one that uses sCO2 cycles along with other conceivable combinations to recover waste heat successfully and efficiently through power, cooling, heating, or freshwater generation.

The main objectives of this research work were to –

I. Construct comprehensive thermodynamic model for basic thermodynamic cycles using python environment.

II. Test the developed models comprehensively and examine the results against published data.

III. Propose a new thermodynamic cycle configurations.

IV. Determine the performance of the proposed configurations. A complete thermodynamic analysis and efficiency evaluation of developed configurations was conducted.

V. Investigate the impact of key operating parameters for developed system

1.4 Contribution of the study

This study proposes a newly conceived combined power and multigeneration cycle, which is considered unique.

1.5 Thesis Organization

Following the brief introduction and explanation of the rationale for the research that was offered in this study in the section before this one, **Chapter 2** covers the history of combined cycle and polygeneration technology and the fundamental background information. This section also provides an in-depth analysis of the efforts made toward obtaining better levels of efficiency and recovering waste heat through the utilization of combined cycle and multiple output generation technology with an emphasis on sCO2 cycles.

In Chapter 3, the approach and procedures that are utilized to construct off-design computational models that were used to acquire the cycle performance findings were described.

A thermodynamic study of a newly designed combined power cycle and polygeneration cycle systems is presented in **Chapter 4.** The purpose of this analysis is to increase the overall thermal efficiency of power cycles and utilizing waste heats.

In Chapter 5, A summary of the most significant findings and outcomes, as well as major conclusions and recommendations for further research were presented.

Chapter 2
LITERATURE REVIEW

The use of low/medium-grade heat in various investigated systems was explored in the literature review. The work of several scientists on the supercritical CO2 recompression cycle, refrigeration cycle, and Kalina cycle using various sources of energy has been mentioned from time to time. A short background of the supercritical CO2 cycle has also been provided, as well as its attributes.

2.1 Sources of Low/ Medium-grade Heat

The ammonia-water Rankine cycle was studied using thermodynamics of finite size by Roy et al. [2]

According to the first two laws of thermodynamics, the ammonia-water Rankine cycle was analyzed by Kim et al. [3], including or excluding regeneration for the restoration of a low power heat source, and the characteristics of the pinch point in the exchangers were explored.

Organic fluids are used in ORCs, while water is used in SRCs. Because the molecular weight of the organic fluids being used ORC systems is greater than the volume, the flow rate of the employed fluid mass increases for the same expander size. As a result, it has the ability to improve efficiency while lowering turbine losses. [4]

The liquefying value of organic fluids permits for the use of limited heat sources as well. [5]

A combination plant with an ammonia-water combination as the working substance was presented by Goswami et al. [6] The system they demonstrated was a hybrid of absorption refrigeration and Rankine cycles.

The thermodynamic performance of the Goswami system was investigated

by Fontalvo et al. [7] and Pouraghaie et al [8]. They demonstrated that the Goswami plant's cooling load is minimal.

Two novel combined cycles were developed by combining two cycles, the absorption refrigeration cycle and the Kalina cycle [9]. They show that their recommended system is more efficient in terms of both electricity and cooling production.

2.1.1 Solar Energy

At lower temperatures (under 400°C), the organic Rankine cycle (ORC) is a particularly advantageous cycle. Several researchers looked on the thermodynamics and technological elements of ORC. [10]

Shaaban conducted a thermodynamic evaluation of a combined cycle which uses solar power in 2016, which included two different bottoming cycles: the steam Rankine cycle (SRC) and the organic Rankine cycle (ORC) [11]. For bottoming ORC, the author experimented with 15 different organic fluids and found that R1234ze(z) is by far the best ideal working liquid in terms of thermally, safety, and environmental considerations.

Al-Sulaiman and Atif [12] looked at how various sCO2 Brayton cycle architectures performed when combined with a tower run by solar energy. With a thermal efficiency of 52 percent, the recompression Brayton cycle looked good.

2.1.2 Geothermal Energy

Geothermal sources have the service offerings across renewable resources since they are not weather-dependent, and advanced biofuels available that permit electricity production using geothermal fluids at relatively low temperature. [13]**.** Several thermodynamic cycles have been studied over the last 20 years. Conceptual studies have indicated the possibility of these innovative cycles, which are made to run by low or medium heat sources.

[14] One of their distinguishing features is that they use a reaction mixture as the liquid to improve thermal efficiency. [6]

The Rankine and Kalina cycles are combined as a bottoming cycle with the identical boundary parameters, El-Sayed and Tribus [15] analyzed them analytically. They ran two laws of thermodynamic calculations and found that Kalina cycle can achieve a 10%–30% better thermal performance than a comparable Rankine cycle.

For geothermal heat sources run by low-temperature, Hettiarachchi [16] evaluate the impacts of the Kalina power cycles 11 (KSC11) with that of an ORC in 2007. The findings demonstrate that for a turbine input pressure, an considerable ammonia proportion may be determined that provides the cycle efficiency of highest value. At low pressures, KSC11 outperforms the organic Rankine cycle in terms of overall efficiency.

2.2 Thermodynamic Cycles to utilize Low/Medium-grade Heat

A significant amount of the power consumed is released into the environment as low/medium grade heat losses in various forms. [17] As a result, repurposing such low/medium grade excess heat for heat-driven cooling or electricity production is critical and urgent. [18], [19]

Chacartegui et al. [20] presented a part-load assessment and a parameterized modification of a cogeneration with a topping cycle of gas turbine and an ORC having low temperature bottoming cycle to obtain better combination of these two cycles. These studies show how the evaporating pressure affects performance, and several of them give a parameterized enhancement and findings assessment of exhaust heat having low-grade sources. [21] [22]

2.3 Combined Cycle Systems

Petrakopoulou et al. [23] used both traditional and innovative exergetic analytic methods to examine a combined - cycle plant. They finished the

exergy analysis while breaking exergy destruction component into controllable, inevitable, internal, and external portions, in addition to the traditional exergy performance study.

Bassily [24] looked at ways to reduce the unsustainability of HRSG in combined cycles, as well as modeling and analyzing latest cooling technologies for industrial combined cycles. Lessen the thermal disparities between pinch points and flow rates of mass including steam drums, per the research, to minimize unsustainability.

The influence of flow rate of mass and input gas heat on the performance of the cycle was investigated by Kaviri et al. [25] They discovered that raising the input temperature has favorable impact on efficiency until it reaches 650 degrees Celsius, but afterwards it seems to have a detrimental impact.

2.4 Polygenerations Systems

Numerous research have lately worked on the concept and evaluation of unique multi-generation setups that use a variety of alternative energy sources. Several outcomes, such as refrigeration, [26] domestic water heating, [27] and hot air, have also been researched by scientists. Low-grade heat streams are used to classify certain new energy resources. When using low-grade heat, the typical power cycle may also not maintain the desired efficiency due to its low thermal efficiency. Supercritical CO2 (hence considered as S-CO2) considered as a potential liquid for power systems, providing great efficiency, excellent stability, and protection.

Ahn et al. [28] offered an overview of the S-CO2 cycle's early stage of growth as well as a comparison of several S-CO2 arrangements in respect of cycle effectiveness.

Dostal et al. [29] did a comparison overview of varieties of sCO2 Brayton cycles and discovered that recompression Brayton cycle result a more

thermal effectiveness of 7%.

Padilla et al. [30] tested the thermal performance of several sCO2 Brayton cycles using a dry coolant. Having a turbine input level of 850°C, the recompression cycle having intercooling result the maximum efficiency around 55.2%.

2.5 Properties of Supercritical CO2

Supercritical fluids, as is well recognized, are an appealing medium for chemical changes from a technological standpoint. Carbon dioxide has special capabilities as a reaction mixture when it reaches supercritical temperatures. Kaupp [31], Savage et al. [32] reviewed supercritical CO2 reactions.

Little variations in pressure cause substantial changes in density, which influences diffusivity, viscosity, dielectric, solvation, and various properties, because compressibility (KT) at the critical and supercritical levels is quite high. Therefore, CO2 in supercritical circumstances are greatly affecting the dynamics and processes of chemical changes, i.e., somebody can alter the response conditions (e.g., solvent characteristics) by changing pressure and temperature. [33]

2.6 History of Supercritical CO2 Cycle

Sulzer Bros invented a condensation of partial amount CO2 Brayton cycle in 1948, which started the history of the sCO2 Brayton cycle. [34] The benefit of carbon dioxide fluid was rapidly recognized, and research into supercritical CO2 cycles began in a number of countries: In the old Russia, Gokhstein and Verhivker [35], in Italy, Angelino [36], and in the United States, Feher [37] and Sulzer Brown – Boveri is the most important among many others in Switzerland.

Chapter 3
METHODOLOGY

3.1 Selection of Software

Modelling performed by means of Python, and CoolProp external library was used for the thermo-physical properties of supercritical CO2, water, and the organic working fluids. For other fluids like air, combustion/exhaust gas, NH3-H20 solution property equations were used to find out the properties of respective state points.

3.2 Power Cycles Configurations, Modelling and Validation

In this section, the basic thermodynamic equations that make up the physical model of different thermodynamic cycle is presented. These are the mass and energy balances for each component that make up the different thermodynamic cycle configuration. The general assumptions that were made for modelling these cycles are as follows:

1. All the processes attain steady state.
2. The temperature and pressure of ambient or environmental condition are 25°C and 1.013 bar, respectively.
3. The cooling water utilized in the configurations is in the environmental condition.
4. The changes in potential and kinetic energies in each of the cycle component are negligible.
5. Pressure losses (except gas turbine cycle) and heat losses in all of the heat exchangers in the cycle layouts and pipelines are neglected.
6. The losses of the flow inside the turbines, pumps, and compressors, are considered using isentropic efficiencies i.e., Expansion and

compression processes of the cycle are adiabatic but non- isentropic

7. Heat transfer for the cycle components with the ambient is negligible.

3.2.1 Gas turbine cycle

The standard gas turbine cycle is depicted schematically in Fig. 3.1. The gas turbine cycle consists of a compressor, a combustion chamber, and a turbine. Assumptions made for modelling gas turbine cycle are as follows:

1. For the pressure loss of the air and gas streams in the combustion chamber and heat exchangers reasonable values are adapted [38][39]

2. The combustion fuel is considered natural gas (methane) having a lower heating value (LHV) of 50,000 kJ/kg

Air at ambient conditions enters the air compressor (point 1) where the compression process takes place to raise the pressure of the air at desired pressure ratio and, after compression process (point 2), the air is then supplied to CC. Combustion fuel is then injected and burnt inside the CC and hot combustion gases that exit attain requisite turbine inlet temperature (point 3) and then pass to GT to produce power through the generator and also drive AC. The hot gas expands in the GT to point 4.

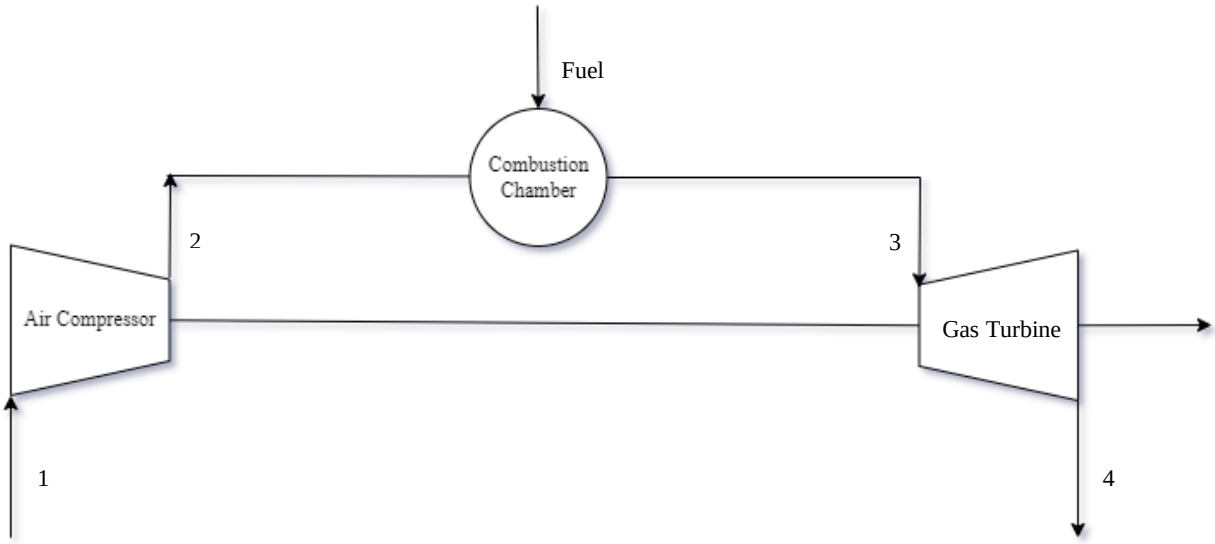

Fig. 3.1 Illustration of conventional gas turbine cycle

3.2.1.1 Modelling

The following are the governing thermodynamic equations and energy balances that are related to the components of the gas turbine cycle: [38]

3.2.1.1.1. Air Compressor

$$T_2=T_1\times\left\{1+\frac{1}{\eta_{AC}}\times\left[\left(\frac{P_2}{P_1}\right)^{\frac{\gamma_a-1}{\gamma_a}}-1\right]\right\},\ P_1=P_o \text{ and } T_1=T_o \tag{3.1}$$

$$\dot{W}_{AC}=\dot{m}_a\times C_{p_{air}}\times(T_2-T_1) \tag{3.2}$$

$$r_p=\left(\frac{P_2}{P_1}\right) \tag{3.3}$$

3.2.1.1.2. Combustion Chamber

$$\dot{m}_{gas}=\dot{m}_{air}+\dot{m}_{fuel} \tag{3.4}$$

$$\dot{m}_{air}h_2 + \dot{m}_{fuel}LHV = \dot{m}_{gas}h_3 + \dot{m}_{fuel}LHV\,(1 - \eta_{CC}) \text{ with } \eta_{CC} = 0.98 \quad (3.5)$$

3.2.1.1.3. Gas Turbine

$$T_4 = T_3 \times \left\{ 1 - \frac{1}{\eta_{GT}} \times \left[1 - \left(\frac{P_3}{P_4} \right)^{\frac{1-\gamma_{gas}}{\gamma_{gas}}} \right] \right\} \quad (3.6)$$

$$\dot{W}_{GT} = \dot{m}_g \times C_{p_{gas}} \times (T_3 - T_4) \quad (3.7)$$

$$\dot{W}_{net.GT} = \dot{W}_{GT} - \dot{W}_{AC} \quad (3.8)$$

3.2.1.1.4. Specific energy of air and gas streams

For air stream (i =1 & 2):

$$\text{enthalpy , } h_i = C_{p_{air}} \times (T_i - T_o) \quad (3.9)$$

For gas stream (i =3 & 4):

$$\text{enthalpy , } h_i = C_{p_{gas}} \times (T_i - T_o) \quad (3.10)$$

The workflow for developing the gas turbine cycle model is illustrated in Fig. 3.2

3.2.1.2 Validation Result

Table 3.1 compares the thermodynamic state of each stream of gas turbine cycle obtained by the presented model and that reported by reference [38]. The table shows very close agreement for the developed model. There is no remarkable difference appeared in the validation result.

Table 3.1 Validation results for gas turbine cycle model

Input Parameters	**Working Fluid Stream**	**Temperature, T (°C)**		**Pressure, P (kPa)**	
		Ref. [38]	**Present work**	**Ref.** [38]	**Present work**
r_p= 8.5234 η_{AC}= 0.8468 η_{GT} = 0.8786 CC inlet temp = 641.13 °C GT inlet temp = 1219.48 °C	AC inlet	25	25	101.3	101.3
	AC outlet	322.36	322.55	1013	1013
	CC inlet	641.13	641.13	962.3	962.35
	GT inlet	1219.48	1219.48	914.2	914.23
	GT outlet	714.75	715.15	109.9	109.93

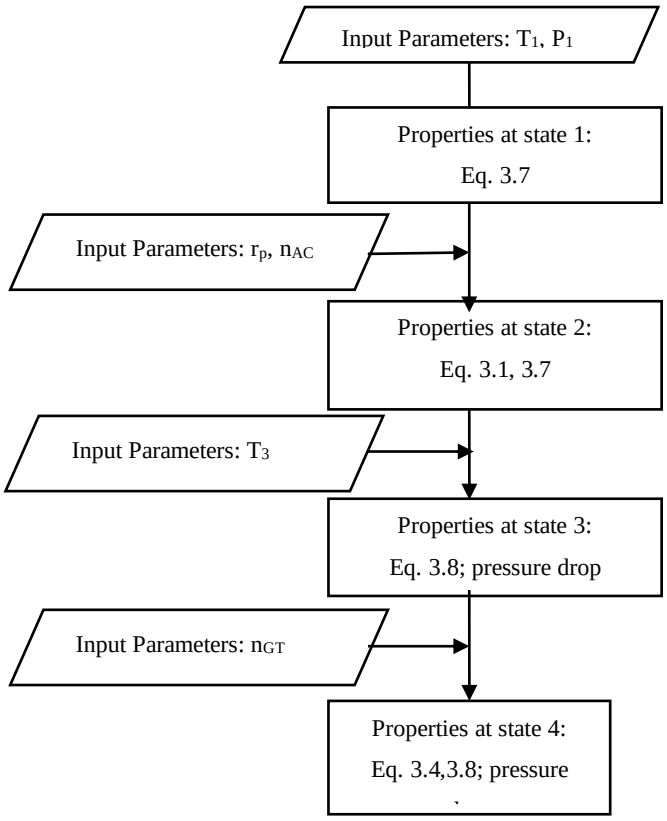

Fig. 3.2 Flowchart of modelling of gas turbine cycle

3.2.2 S-CO2 Power Cycle

The s-CO2 cycle configuration considered for this study is recompression due to their high efficiency and simple layout. The cycle is illustrated in Fig. 3.3 cycle which also includes one stage of reheat.

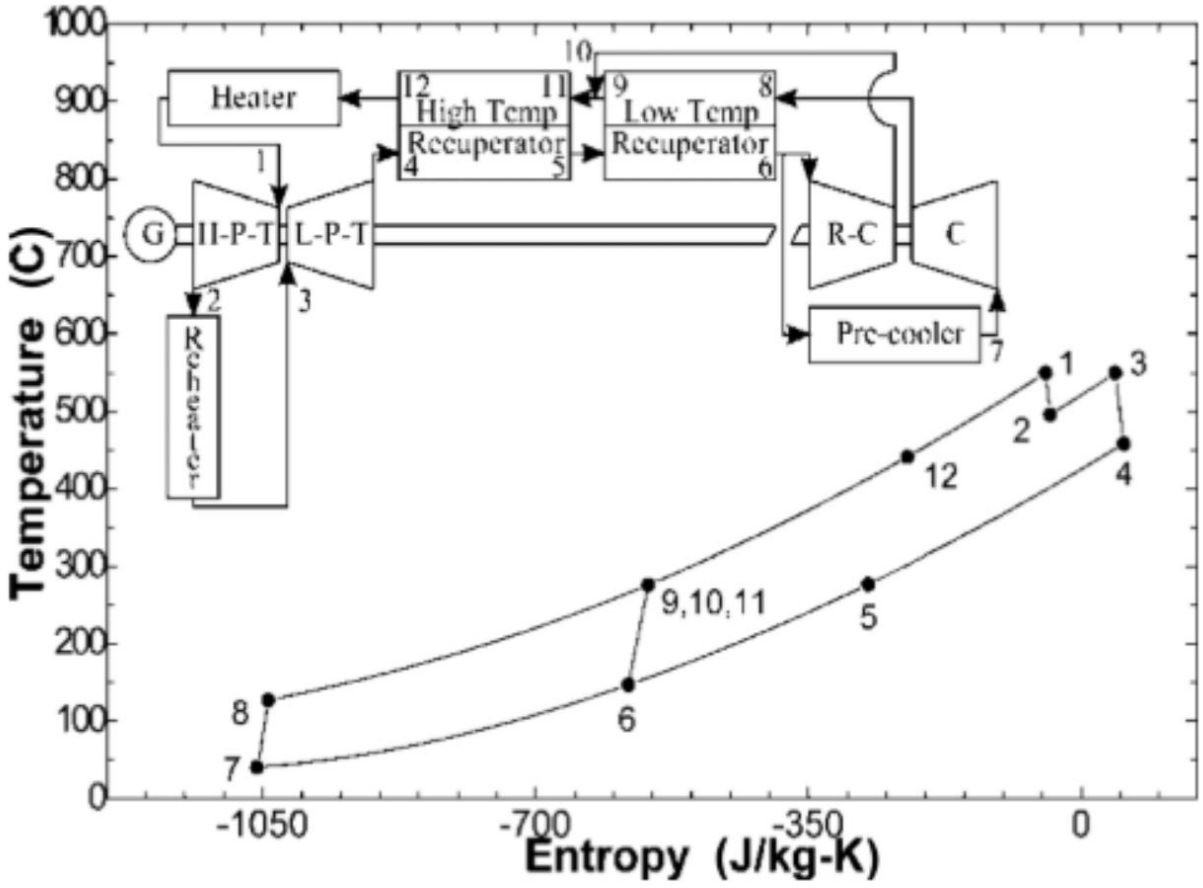

Fig. 3.3 Recompression Brayton cycle with reheat layout and temperature-entropy diagram [40]

3.2.2.1 Standalone Cycle Modelling

The followings are the governing thermodynamic equations and energy balances that are related to the components of recompression sCO2 Brayton cycle:

3.2.2.1.1. Turbomachinery modelling

The compressors (η_c) and turbines (η_t) isentropic efficiency are defined as follows:

$$\eta_c = \frac{h_{out_{isen}} - h_{in}}{h_{out} - h_{in}} \tag{3.11}$$

$$\eta_t = \frac{h_{in} - h_{out}}{h_{in} - h_{out_{isen}}} \tag{3.12}$$

Here, h_{in} and h_{out} are the actual inlet and outlet enthalpies, respectively, and $h_{out_{isen}}$ is the isentropic outlet enthalpies

The turbomachinery outlet properties are obtained using following two equations:

$$h_{out_{isen}} = (P_{out}, s_{out_{isen}}) \tag{3.13}$$

$$s_{in} = s_{out_{isen}} \tag{3.14}$$

Pressures at any state can be calculated using following equation

$$PR = \frac{P_{high}}{P_{low}} \tag{3.15}$$

After calculating specific isentropic outlet enthalpy with equation (3.13), the actual enthalpy can be obtained using the isentropic efficiency equation (3.11). The specific actual work is calculated as

$$w = h_{in} - h_{out} \tag{3.16}$$

3.2.2.1.2. Recuperator modelling

HTR and LTR effectiveness are calculated as [39]

$$\varepsilon = \frac{h_{rh_{in}} - h_{rh_{out}}}{h_{rh_{in}} - h(P_{rh_{out}}, T_{rc_{in}})} \tag{3.17}$$

where h is enthalpy, P is pressure, T is temperature and The term "cold side of the recuperator" is denoted with the subscript "rc," whereas "hot side of the recuperator" is denoted with the subscript "rh." in and out are subscripts that indicate the conditions at the intake and outlet, respectively.

3.2.2.1.3. Other thermodynamic relations

$$h_{12} - h_{11} = h_4 - h_5 \tag{3.18}$$

$$(1\text{-}x)\ (h_9\text{-}h_8) = (h_5\text{-}h_6) \tag{3.19}$$

Where, x is recompressed mass flow ratio

CoolProp external library was used for the thermo-physical properties of supercritical CO2.

3.2.2.2 Validation

Table 3.2 compares the data obtained using presented modelling approach to that of reference [41] for supercritical CO_2 recompression Brayton cycle with reheat. The table shows very close agreement for the developed model.

Table 3.2 Cycle comparison with Dostal [41]

Input Parameters	**Turbine Inlet Temperature, T (°C)**	**Efficiency**		**Percentage error, %**
		Ref. [41]	**Present work**	
Turbine Inlet temperature = 500°C -850°C P_r = 2.0 – 9.0 Main compressor outlet pressure = 25 MPa Main compressor inlet temperature = 32°C Compressor efficiency = 89 % Turbine efficiency = 93 % (To match with [41], turbine efficiency is assumed 90% for the recompression cycle [40]) LTR & HTR effectiveness = 95%	500	44.40	45.26	1.94
	550	46.49	47.18	1.48
	600	48.24	48.83	1.22
	650	49.93	50.26	0.66
	700	51.40	51.51	0.21
	750	52.69	52.62	0.13
	800	53.87	53.60	0.50
	850	54.9	54.48	0.77

Fig. 3.4 shows the workflow for recompression cycle model

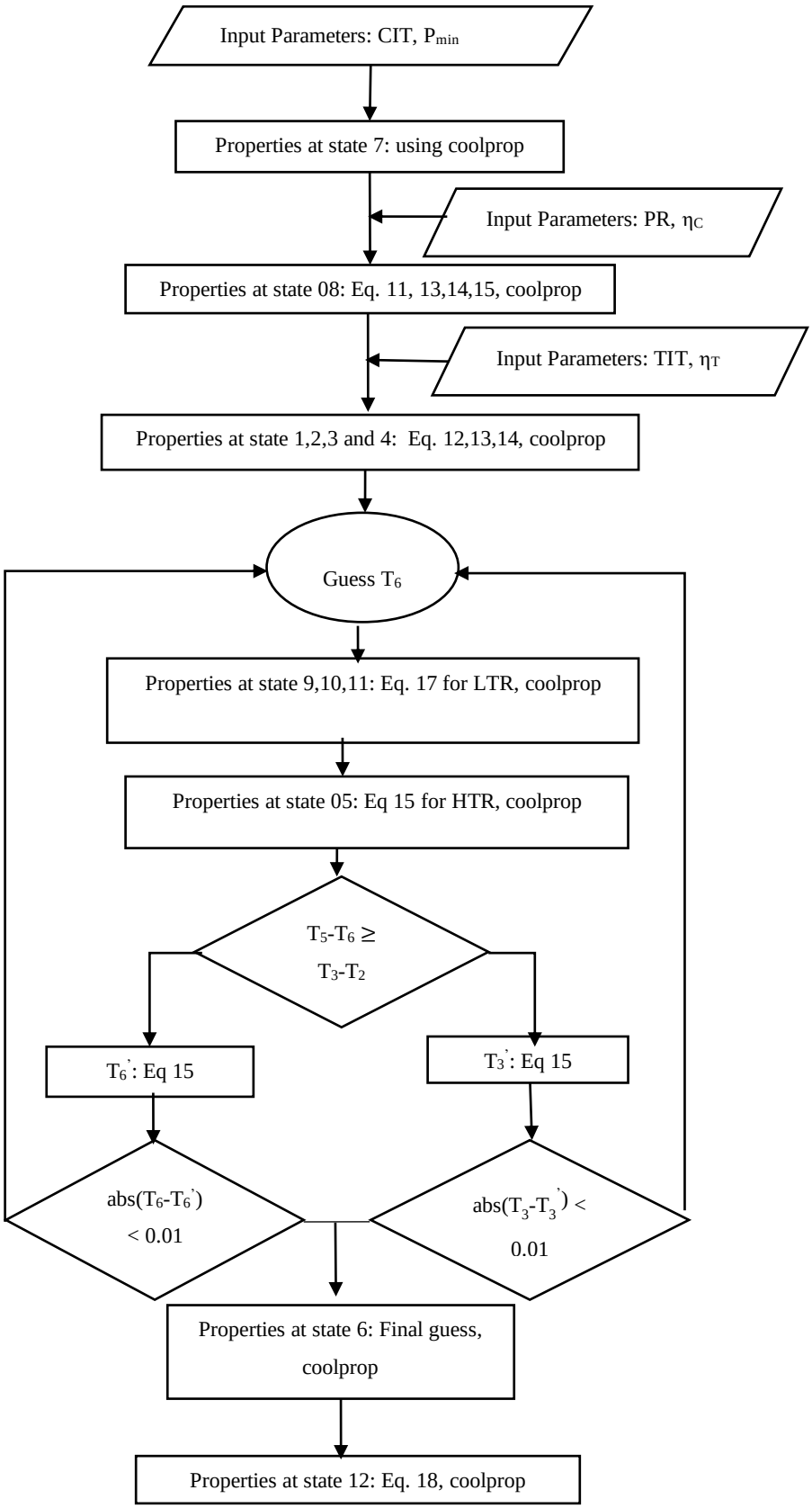

Fig. 3.4 Flowchart of modelling of recompression cycle

3.2.3 NH_3-H_2O Absorption Refrigeration Cycle

The H_2O-LiBr cycle and the NH_3-H_2O cycle are the two most frequent types of absorption systems. When compared to H_2O, the refrigerant NH3 has the benefit of being able to evaporate at temperatures that are lower range from -10 to 0 degrees Celsius, as opposed to temperatures that range from 4 to 10 degrees Celsius. As a result, the NH3-H2O cycle is utilized in the refrigeration process. The essential components of the absorption refrigeration cycle are depicted in Fig. 3.5. The high-pressure liquid refrigerant in the condenser (2) enters the evaporator (4) by means of an expansion valve (3), which brings the pressure of the refrigerant down to the lower level that is present in the evaporator. The weak solution is formed when the liquid refrigerant (3) absorbs heat from the material that is being cooled in the evaporator, and the resulting low-pressure vapor (4) travels to the absorber, where it is absorbed by the strong solution from the generator (8) via an expansion valve (10). After the refrigerant has been removed by boiling, the weak solution (5) is pumped up to the generating pressure (7). When the remaining solution (8) flows back to the absorber, the cycle is said to have been completed.

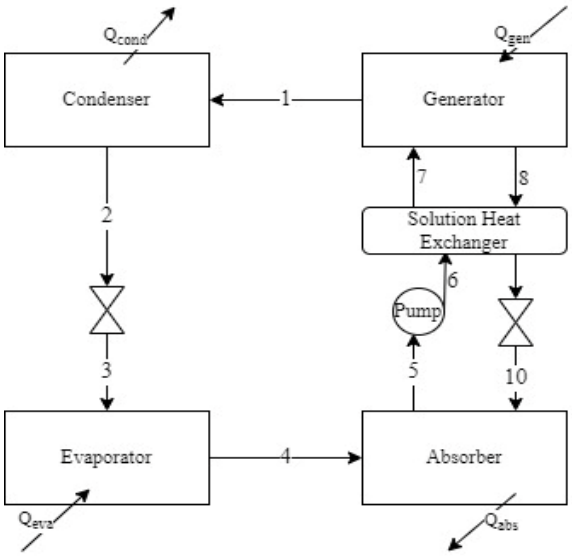

Fig. 3.5 The schematic of the absorption refrigeration cycle

3.2.3.1 Modelling

For the generator, the mass and energy balances yield:

$$m_7 = m_1 + m_8 \text{ (Total mass balance)} \tag{3.20}$$

$$m_7 X_7 = m_1 + m_8 X_8 \text{ (NH_3 mass balance)} \tag{3.21}$$

$$Q_{gen} = m_1 h_1 + m_8 h_8 - m_7 h_7 \tag{3.22}$$

From equations (3.21) and (3.22), the strong and weak solutions mass flow rates are determined by:

$$m_8 = \frac{1 - X_7}{X_7 - X_8}\, m_1 \tag{3.23}$$

$$m_7 = \frac{1 - X_8}{X_7 - X_8}\, m_1 \tag{3.24}$$

The energy balance for the solution heat exchanger is as follows:

$$T_9 = \varepsilon_{SHE} T_6 + (1 - \varepsilon_{SHE}) T_8 \tag{3.25}$$

$$h_7 = h_6 + \frac{m_8}{m_6}(h_8 - h_9) \tag{3.26}$$

For the pump:

$$h_6 = h_5 + (P_6 - P_5)v_6 \quad (3.27)$$

$$W_{pump} = (P_6 - P_5)v_6 \quad (3.28)$$

energy balances for the absorber, condenser and evaporator is given by following equations respectively:

$$Q_{abs} = m_4 h_4 + m_{10} h_{10} - m_5 h_5 \quad (3.29)$$

$$Q_{cond} = m_1(h_1 - h_2) \quad (3.30)$$

$$Q_{eva} = m_1(h_4 - h_3) \quad (3.31)$$

If the temperatures of the generator, condenser, absorber, and evaporator as well as the refrigerant mass flow rate or the needed refrigerating load are known, then the equations described above can be solved concurrently to determine the performance of the system.

3.2.3.2 Thermodynamic properties of NH_3 refrigerant and NH_3-H_2O solution

The thermodynamic properties at states (1)-(4) in Fig. 3.5 are determined by NH_3, and but properties at states (5)-(10) can be calculated based on the binary mixture of NH_3-H_2O solutions. Coolprop library could not determine the thermodynamic properties of of NH_3 refrigerant and NH_3-H_2O solution. Thus, property relations adapted from ref [42] are modelled to find out the state points of refrigeration cycle.

3.2.3.2.1. Refrigerant NH_3

Both the pressure and the temperature of the two-phase equilibrium of the

refrigerant NH3 are connected by the following relation:

$$P(T) = 10^3 \sum_{i=0}^{6} a_i (T - 273.15)^i \tag{3.32}$$

The followings are expressions of the specific enthalpies of NH3's liquid and vapor states, both of which are saturated, in terms of temperature:

$$h_{liquid}(T) = \sum_{i=0}^{6} b_i (T - 273.15)^i \tag{3.33}$$

$$h_{vapor}(T) = \sum_{i=0}^{6} c_i (T - 273.15)^i \tag{3.34}$$

Table 3.3 provides the list of coefficients of equations (3.32) - (3.34)

Table 3.3 Coefficients of two-phase equilibrium pressure and temperature relation and enthalpy of saturated liquid and vapor relations

i	**a_i for equation (3.32)**	**b_i for equation (3.33)**	**c_i for equation (3.34)**
0	4.2871×10^{-1}	1.9879×10^{2}	1.4633×10^{3}
1	1.6001×10^{-2}	4.4644×10^{0}	1.2839×10^{0}
2	2.3652×10^{-4}	6.2790×10^{-3}	-1.1501×10^{-2}
3	1.6132×10^{-6}	1.4591×10^{-4}	-2.1523×10^{-4}
4	2.4303×10^{-9}	-1.5262×10^{-6}	1.9055×10^{-6}
5	-1.2494×10^{-11}	-1.8069×10^{-8}	2.5608×10^{-10}

6	1.2741×10^{-13}	1.9054×10^{-10}	-2.5964×10^{-10}

3.2.3.2.2. NH_3-H_2O solution

The following equation illustrates the relationship between the saturation pressure and temperature of an ammonia-water mixture:

$$\log P = A - \frac{B}{T} \tag{3.35}$$

Where ,

$$A = 7.44 - 1.767\,X + 0.9823\,X^2 + 0.3627X^3 \tag{3.36}$$

$$B = 2013.8 - 2155.7\,X + 1540.9\,X^2 - 194.7\,X^3 \tag{3.37}$$

The following is a relationship that may be drawn between enthalpy, temperature, and concentration, with coefficients provided in Table 3.4

$$h(T,\bar{X}) = 100 \sum_{i=0}^{16} a_i \left(\frac{T}{273.15} - 1\right)^{m_i} \bar{X}^{n_i} \tag{3.38}$$

where, $\bar{X}$ is the ammonia mole fraction and related as follows with concentration:

$$\bar{X} = \frac{18.015\,X}{18.015\,X + 17.03\,(1 - X)} \tag{3.39}$$

Table 3.4 Coefficients of temperature, concentration and enthalpy relation of NH_3-H_2O Solution

i	**m_i**	**n_i**	**a_i**	**i**	**m_i**	**n_i**	**a_i**
1	0	1	-7.6080×10^0	9	2	1	2.84179×10^0
2	0	4	2.56905×10^1	10	3	3	7.41609×10^0
3	0	8	-2.47092×10^2	11	5	3	8.91844×10^2
4	0	9	3.25952×10^2	12	5	4	-1.61309×10^3
5	0	12	-1.58854×10^2	13	5	5	6.22106×10^2
6	0	14	6.19084×10^1	14	6	2	-2.07588×10^2
7	0	0	1.14314×10^1	15	6	4	-6.87393×10^0
8	1	1	1.18157×10^0	16	8	0	3.50716×10^0

The relationship that exists between a specific volume, temperature, and concentration.:

$$v(T,X) = \sum_{j=0}^{3}\sum_{i=0}^{3} a_{ij}(T - 273.15)^i X^j \tag{3.40}$$

Table 3.5 provides a list of the coefficients.

Table 3.5 Coefficients of relation among specific volume, temperature and concentration of NH_3-H_2O Solution

i	j	a_{ij}	i	j	a_{ij}
0	0	9.9842×10^{-4}	0	2	-1.2006×10^{-4}
1	0	-7.8161×10^{-8}	1	2	-1.0567×10^{-5}
2	0	8.7601×10^{-9}	2	2	2.4056×10^{-7}
3	0	-3.9076×10^{-11}	3	2	-1.9851×10^{-9}
0	1	3.5489×10^{-4}	0	3	3.2426×10^{-4}
1	1	5.2261×10^{-6}	1	3	9.8890×10^{-6}
2	1	-8.4137×10^{-8}	2	3	-1.8715×10^{-7}
3	1	6.4816×10^{-10}	3	3	1.7727×10^{-9}

3.2.3.3 Validation

Table 3.6 provides the comparison between the thermodynamic properties of each stream of refrigeration cycle obtained by the present model and that reported by reference [42]

Table 3.6 Validation results for absorption refrigeration cycle model

Input Parameters	**Working Fluid State**	**Temperature, T (°C)**		**Pressure, P (kPa)**		**NH3 concentration, X (%)**	
		Ref. [42]	**Present work**	**Ref.** [42]	**Present work**	**Ref.** [42]	**Present work**
T_{gen} = 100 °C T_{cond} = 30 °C T_{abs} = 25 °C T_{eva} = -5 °C Effectiveness of the solution heat exchanger of 80%	Generator NH_3-vapor exit	100	100	1166.92	1166.92	100	100
	Condenser NH_3-Liquid exit	30	30	1166.92	1166.92	100	100
	Evaporator NH_3-vapor exit	-5	-5	354.42	354.42	100	100
	Absorber solution exit	25	25	354.42	354.42	52.24	52.63
	Generator solution inlet	67.70	65.95	1166.92	1166.92	52.24	53.63
	Generator solution exit	100	100	1166.92	1166.92	33.55	33.52
	Absorber solution inlet	40	40	354.42	354.42	33.55	33.52

Fig. 3.6 shows the workflow for absorption refrigeration cycle model

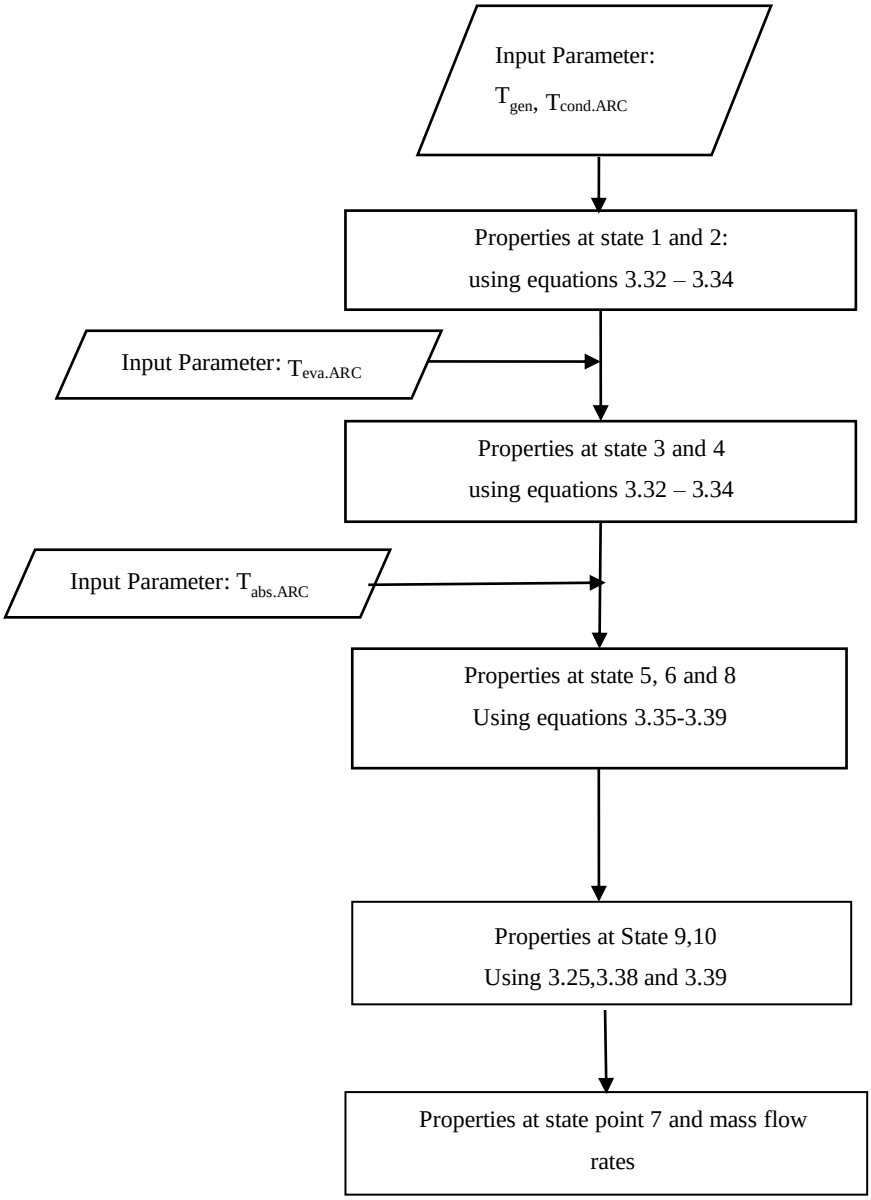

Fig. 3.6 Workflow of modelling of absorption refrigeration cycle

3.2.4 Other available power cycles models

Other power cycles include the fundamental Brayton cycle and its different layouts, the Rankine cycle, and its various configurations, organic rankine cycle models were also constructed for the aim of simulating diverse power cycles. And confidence developed for the subsequent action.

3.3 Selection of Scenario/Configuration of Current Study

After analyzing and modeling standalone cycles, the next objective was to study and construct models for various configurations of combined cycle systems and polygeneration systems that emphasize the sCO_2 cycle. The S-The CO2 Brayton cycle may be coupled with a number of different cycles to create a more sophisticated system. The exhaust temperature of a gas turbine is roughly 773–873 K. The S-CO2 Brayton cycle may be employed as the bottoming cycle of a gas turbine in order to decrease the ultimate exhaust temperature and improve energy efficiency by utilizing the turbine's waste heat in stages [43]. Adding a bottoming cycle to the sCO2 cycle such as a transcritical CO2 (T-CO2) Brayton cycle [44] or an ORC [45] can further improve the efficiency of an S-CO2 Brayton cycle to a significant extent. It is therefore regarded a viable primary mover for CCHP systems because of its potential to deliver better efficiency in a wider operating temperature range and to apply to a variety of heat sources, as well as to increase the system's dependability. Again, some research has been done on the topic of recovering waste heat from an S-CO2 Brayton power cycle by including a Kalina cycle and making use of an absorption absorption refrigeration cycle (ARC) [46]. Models for these systems were also developed and verified.

Following a thorough investigation utilizing waste heats of gas turbine and sCO2 power cycle, the following combined and multiple generation systems of study were developed.

3.4 Developed Novel Configurations

3.4.1 Configuration -1

Fig. 3.7 illustrates the schematic diagram of the newly developed combined cycle system which includes a gas turbine cycle, an organic Rankine cycle, and supercritical CO2 recompression Brayton cycle with reheat which is integrated with an absorption refrigeration cycle.

Air at ambient conditions is drawn into the air compressor (point 1), which then initiates the compression process to raise the pressure of the air to the appropriate pressure ratio. Following compression (point 2), the air is then provided to CC. In the CC, fuel is injected and burned, and then the hot combustion gases depart, reaching the required temperature for the turbine inlet (point 3). They then go on to the GT, where they are used to produce electricity through the generator, which drives the AC. The hot gas continues to grow all the way to point 4 in the GT. The organic Rankine cycle and the supercritical CO2 recompression cycle both get their heat from the same source: hot flue gas.

The high-temperature exhaust (point 4) that is discharged from the GT first enters the heat HE, where it heats the supercritical CO2 (which is the working fluid for the supercritical CO2 recompression cycle) that is coming out of the HTR (point 04), in order to reach the inlet temperature of the HPT (point 05) of the supercritical CO2 recompression cycle. In order to generate work, the heated sCO2 is allowed to expand until it reaches a pressure that is equivalent to the midway (point 06) of the HPT intake. The liquid next goes via the reheater, where it is heated once more to the maximum temperature of the cycle (point 07), and then it enters LPT. The low-pressure sCO2 then flows (point 09) to the LTR (low temperature recuperator) to heat the high-pressure sCO2 stream (03), after which it departs the low-pressure turbine and enters the high-temperature recuperator as the hot stream (point 08).

This heats the high-pressure sCO2 stream (03). Stream 010a and stream 010b are the names given to the two branches of the sCO2 stream that may be found emerging from the LTR in state 010. The stream 010a, which has a larger mass flow rate, goes into the generator to reject some of the heat to the bottoming ARC. After that, it goes (011) to the pre-cooler before being compressed (01) in the main compressor, and after that, it goes (02) into the LTR to be heated for the first time. After being compressed in the RC and combined with the other CO2 stream coming from the LTR, the stream 010b, which has a lower mass flow rate than the other stream, is discharged (03).

Within the generator of the ARC, the weak solution that is at state 007 is able to absorb heat from the waste flue gas that is flowing through stream 010a. The heat causes the refrigerant in the solution to boil off, and it then flows to the condenser (001). The liquid that is left over transforms into strong solution, which then flows (008) into the SHE, which heats the weak solution that is discharged from the pump (006) to achieve the generator weak solution state (007). Moving through the condenser, the vapor refrigerant (001) is converted to a high-pressure saturated liquid at point 002. After that, the low-pressure liquid refrigerant is allowed to flow into the evaporator while the high-pressure liquid refrigerant is restricted across the expansion valve. This brings the pressure of the liquid refrigerant down to the low pressure (003). The low-pressure saturated vapor refrigerant state (state 004) is created when the liquid refrigerant (state 003) absorbs heat from the materials or substances that are being cooled in the evaporator. This causes the liquid refrigerant to evaporate. Through the SHE (009) and an expansion valve (010), the saturated vapor refrigerant (004) is brought into the absorber, where it is to be absorbed by the strong solution that is being produced by the generator (008). This process results in the formation of the weak solution (state 005). After the heat from the SHE is absorbed by the

weak solution, it is pumped up to the pressure of the generator (state 006), after which it flows to the generator to complete the cycle.

The exhaust gas that is released from the HE then travels to the evaporator of the ORC, where it is used to heat and boil the organic working fluid that is discharged from the pump (0004) of the ORC. In order to generate electricity, the ORC turbine uses the expanded heated saturated organic working fluid vapor (0001) as its working fluid. Before being sent through the ORC pump's compression process, the expanded organic working fluid (0002) goes via the condenser to be cooled down and turned into a saturated liquid (0003).

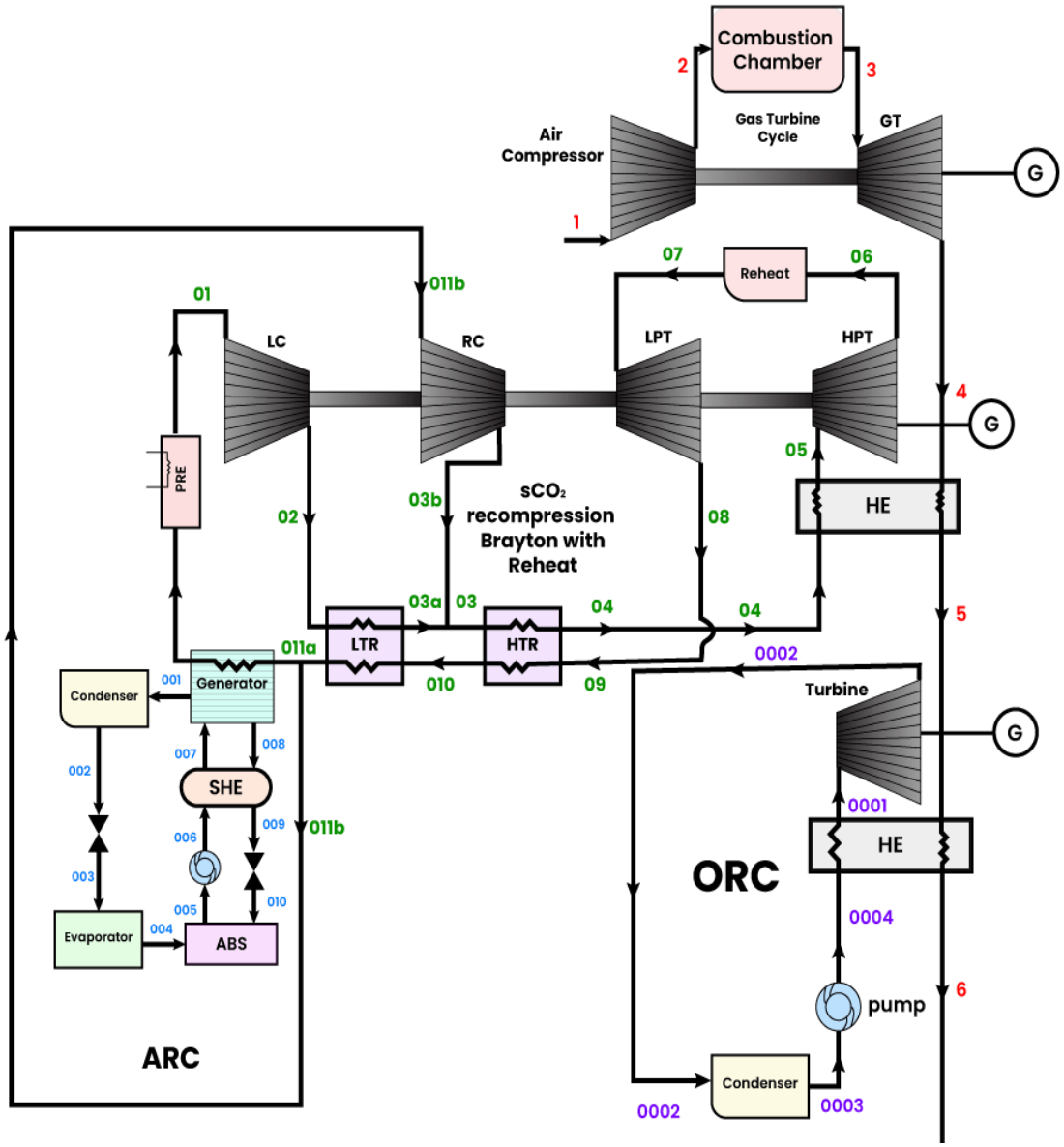

Fig. 3.7 Schematic diagram of the proposed configuration -1

3.4.1.1 Modelling

The standalone cycles were modelled using the equations stated for standalone cycles. For system integration following approach was adapted:

Thermodynamic model of combined gas turbine and organic Rankine cycle is constructed based on Ref. [47]

The maximum amount of heat that can be recovered from the exhaust gases of HE

$$\dot{Q}_{max}=\dot{m}_{gas} \times C_{p_{gas}} \times (T_5-T_{0004}) \quad (3.41)$$

The temperature of the organic working fluid when it is introduced into the evaporator is denoted by T_{0004}

Actual energy that can be used in the evaporator from the HE exhausts gases

$$\dot{Q}_{max}=\varepsilon_{eva} \times \dot{Q}_{act} \quad (3.42)$$

Here, ε_{eva} is evaporator effectiveness

The temperature of the exhaust gas which is leaving the evaporator, T_6, can be estimated using following equation:

$$T_4=T_3-\frac{\dot{Q}_{act}}{\dot{m}_{gas} \times C_{p_{gas}}} \quad (3.43)$$

The mass flow rate of the organic working fluid can be found by:

$$\dot{m}_{ORC}=\frac{\dot{Q}_{act}}{(h_{0001}-h_{0004})} \quad (3.44)$$

The inlet temperature differences for ingoing gases in the heat exchanger (HE) is expressed as:

$$\Delta T_{in}= T_4-T_{05} \quad (3.45)$$

The outlet temperature differences for outgoing gases from the heat exchanger (HE) is expressed as:

$$\Delta T_{out} = T_5 - T_{04} \quad (3.46)$$

The temperature differences in the generator of ARC are calculated as:

$$\Delta T_{gen.hot} = T_{010} - T_{gen} \quad (3.47)$$

$$\Delta T_{gen.cold} = T_{011} - T_{007} \quad (3.48)$$

Fig. 3.8 shows the workflow for developed model

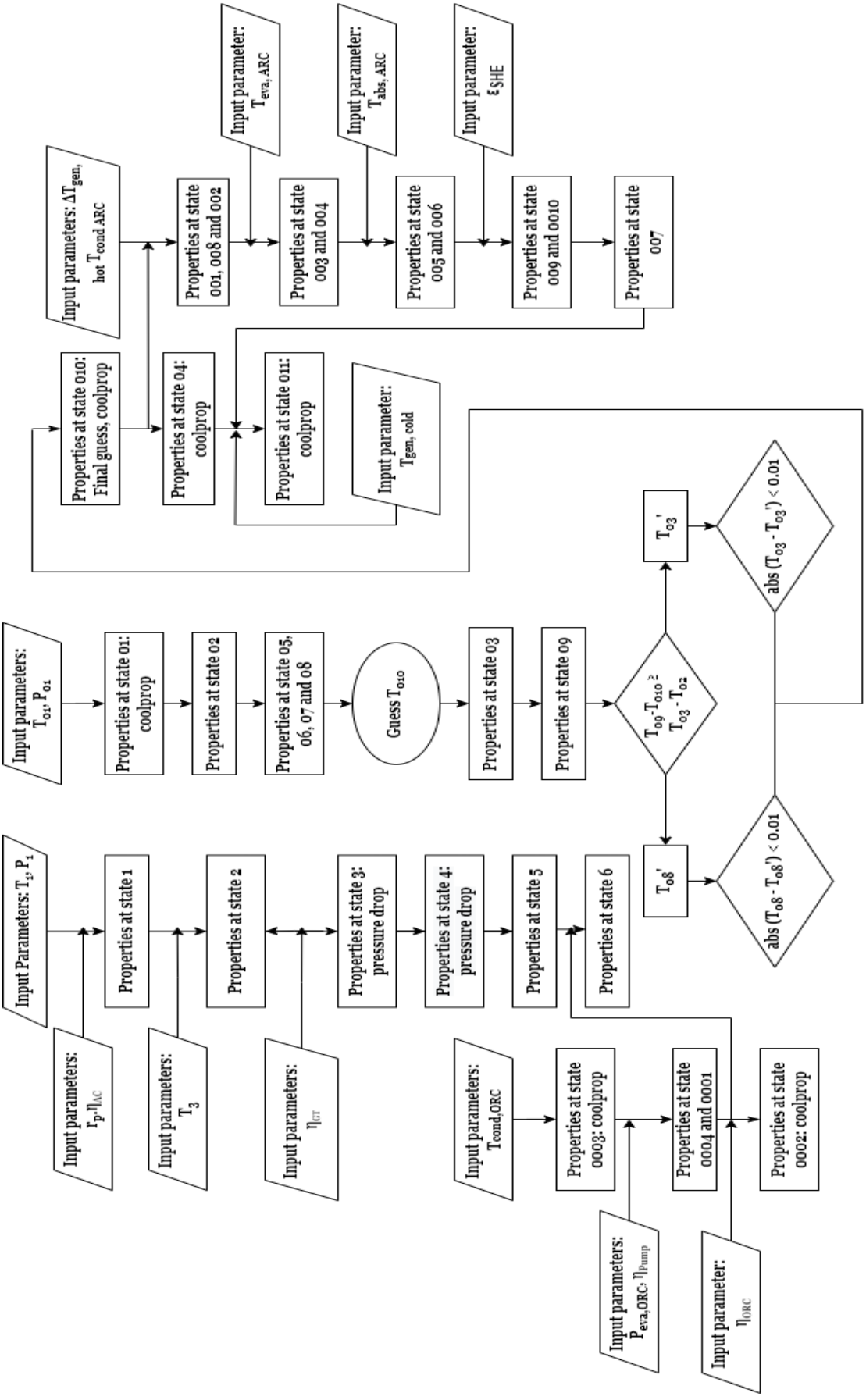

Fig. 3.8 Workflow of modelling of newly derived configuration

3.4.1.2 Parameters that influence cycle performances

The net power generated of the developed combined system is obtained by following equation:

$$\dot{W}_{net.comb} = \dot{W}_{GT} + \dot{W}_{HPT} + \dot{W}_{LPT} + \dot{W}_{T.ORC} - \dot{W}_{AC} - \dot{W}_{RC} - \dot{W}_{MC} - \dot{W}_{PUMP.ARC} - \dot{W}_{PUMP.ORC} \quad (3.49)$$

In this configuration, the first law efficiency is regarded as energy utilization factor (EUF) can be represented as:

$$\mathrm{EUF} = \frac{\dot{W}_{net.comb} + \dot{Q}_{ARC.eva}}{\dot{Q}_{CC} + \dot{Q}_{reheat}} \quad (3.50)$$

The system's cooling performance is measured by the coefficient of performance (COP):

$$COP = \frac{Q_{eva}}{Q_{gen}} \quad (3.51)$$

The net refrigeration effect of the whole system is obtained by following equation:

$$Q_{eva} = m_1(h_{004} - h_{003}) \quad (3.52)$$

3.4.1.3 Selection of decision variables and their ranges

The constraints of the decision variables are adapted from different literature presented in Table 3.7

Table 3.7 Practical constraints of decision variables

Decision Variable	**Range**
Gas Turbine Cycle [48]	
r_p	6-20
η_{GT} (%)	78-91
η_{AC} (%)	72-89
T_3 (K)	1320-1550
Combined sCO_2 Cycle and Absorption Refrigeration Cycle [46]	
PR	2.0 – 4.0
$\Delta T_{gen,hot}$ (°C)	10-45
$\Delta T_{gen,cold}$ (°C)	3-15
$T_{eva,ARC}$ (°C)	-2.9 to 10
ORC	
$P_{eva,orc}$ (MPa)	0.5-3.0(critical pressure)
HE [49]	
ΔT_{in} (°C)	10-100
ΔT_{out} (°C)	10-100

The basic input or fixed parameters assumed for the simulation are summarized in Table 3.8. These values are also adapted from different studies.

Table 3.8 Assumed input value for the configuration

Parameter	Value
P_0 (MPa)	0.1013
T_0 (°C)	25
$C_{p,air}$ (kJ/kgK)	1.004
$C_{p,comb,gas}$ (kJ/kgK)	1.17
R_{air} (kJ/kgK)	0.287
R_{gas} (kJ/kgK)	0.290
T_{01} (°C)	32
$P_{min,sCO2}$ (MPa)	7.4
η_t	0.90
η_c	0.85
ε_{LTR}	0.86
ε_{HTR}	0.86

$T_{cond,ARC}$ (°C)	33
$T_{abs,ARC}$ (°C)	33
$T_{eva,ARC}$ (°C)	0
ε_{SHE}	0.80
$\eta_{t,ORC}$	0.80
η_{pump}	0.80
$\varepsilon_{eva,ORC}$	0.7
$T_{cond,ORC}$ (°C)	30

Chapter 4
THERMODYNAMIC ANALYSIS, RESULT AND DISCUSSION

In this part of the thesis, the findings of this work are analyzed graphically. Parametric analysis of the decision variables gas turbine pressure ratio, inlet temperature of gas turbine, isentropic efficiencies of air compressor, isentropic efficiencies of the gas turbine, recompression cycle pressure ratio, temperature difference in the hot side of generator of ARC, difference in temperature in the cold side of generator of ARC, evaporator temperature of ARC and evaporator pressure of ORC has been done.

4.1 Parametric Analysis of Configuration -1

4.1.1 Impact of Gas turbine pressure ratio

The W_net of combined system rises progressively, however the COP of the system decreases dramatically when the pressure ratio for the gas turbine

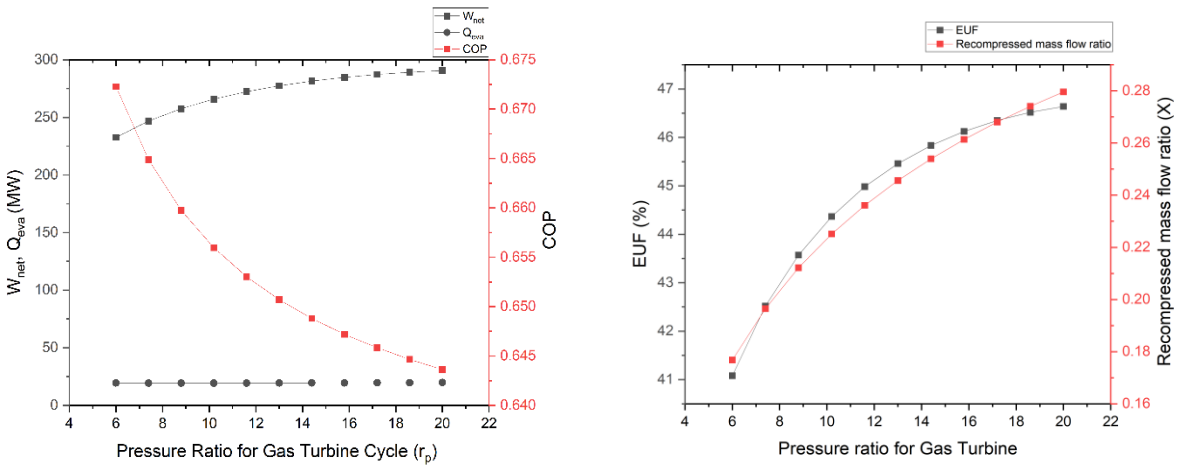

Fig. 3.9 Impacts of Gas turbine pressure ratio on overall performance parameters (EUF, COP, Wnet, Qeva, X)

cycle increases, as shown in Fig. 3.9. The system's Q_eva, however, does not alter.

On the other hand, as the pressure ratio of gas turbine cycle grows, the EUF of the combined system and also the recompression mass flow ratio rises significantly. Inside the studied range, the recompression mass flow ratio approaches 0.28, and the maximum value of EUF is around 47 %.

4.1.2 Impact of inlet temperature of gas turbine

The temperature of the turbine inlet varies between 1320 and 1550 C. The graphs in Fig. 3.10 demonstrate that as the inlet temperature of turbine rises,

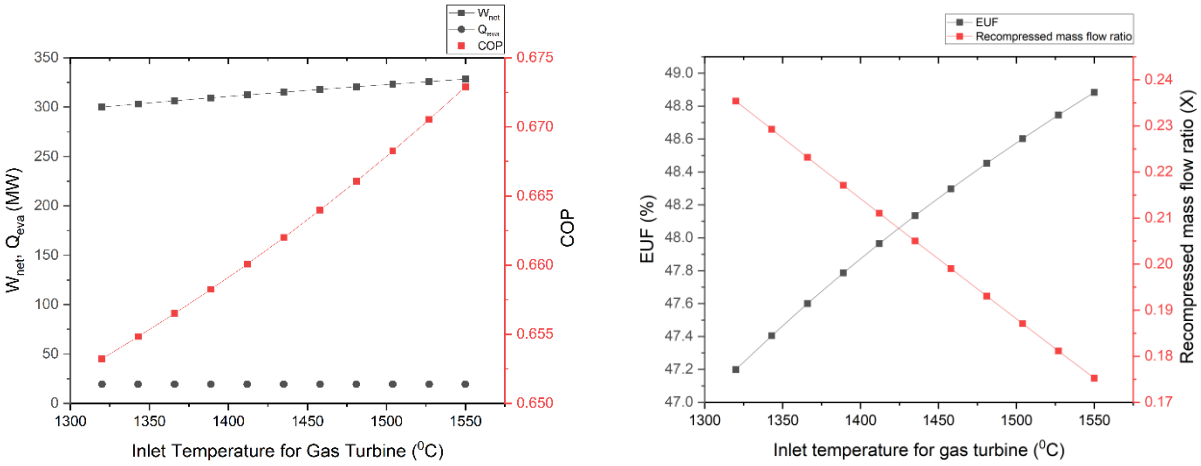

Fig. 3.10 Impact of inlet temperature of gas turbine on overall performance parameters

the net total power output rises as well. This is related to the reasons that the enthalpy loss across the sCO2 turbine rises as the turbine inlet temperature rises, increasing the topping cycle's total power output. The COP of combined cycle also increases drastically with the increment of the temperature of the turbine inlet.

It's worth noting that when the turbine temperature rises, the EUF rises and the recompression flow rate of mass falls. These findings suggest that raising the turbine inlet temperature enhances the combined SCRB/ARC cycle's thermodynamic performance. W_net of the combined cycle grows as temperature of the turbine inlet increases, whereas Q_eva reduces

marginally.

Furthermore, as the temperature of the turbine inlet rises, the rise in W net outweighs the decrease in Q eva. As a result, as the temperature of the turbine inlet rises, EUF rises as well.

4.1.3 Impact of isentropic efficiencies of the air compressor

The COP as well as Q_eva of the combined system remain steady at roughly

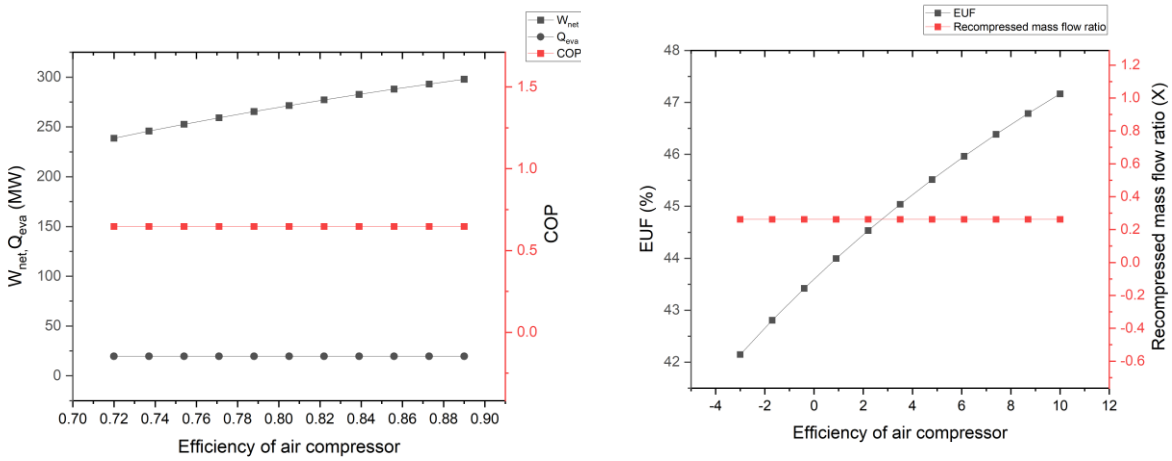

Fig. 3.11 Impact of isentropic efficiencies of the air compressor on overall performance parameters

0.6 and 25MW, respectively, as the air compressor isentropic efficiency rises in Fig. 3.11. W_net, on the other hand, appears to be increasing over time.

The combined system's recompression mass flow ratio remained stable as the isentropic efficiency of the air compressor improved, while EUF increased dramatically, exceeds the threshold figure of more than 47%.

4.1.4 Effect of isentropic efficiencies of the gas turbine

According to graph 3.12, improving the isentropic efficiency of a gas turbine results an increase of W_net of roughly 300MW. The system's COP decreased linearly, whereas Q_eva held steady.

The combined system's EUF and recompression mass flow ratios rise linearly in a similar manner. Because the gradient is so steep, the value

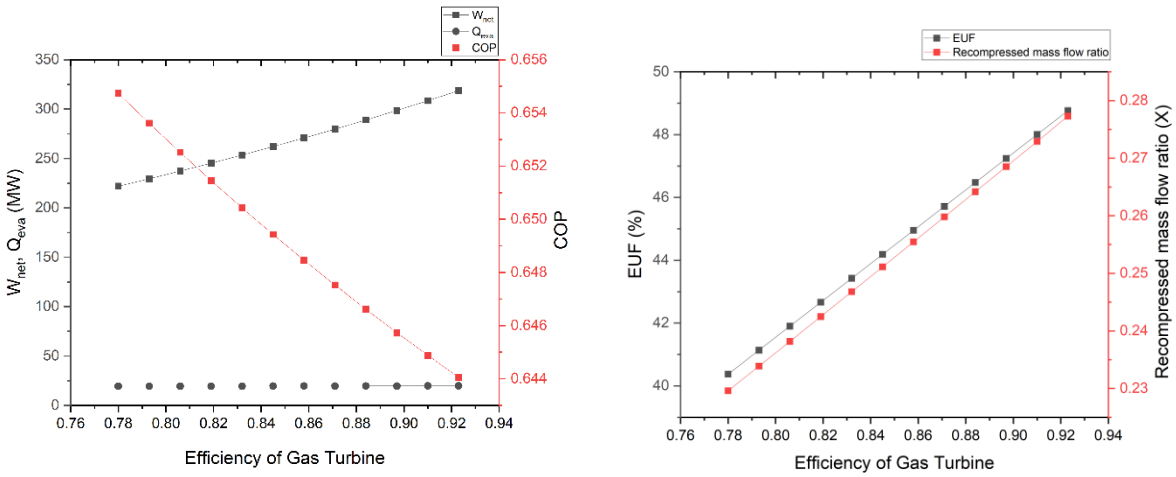

Fig. 3.12 Effects of isentropic efficiencies of the gas turbine on overall performance parameters

quickly rises. The maximal EUF value is around 49%, while the recompression mass flow ratio is around 0.28.

4.1.5 Impact of Pressure ratio of recompression cycle

The total output power climbs to a peak and then drops as PR rises. Because

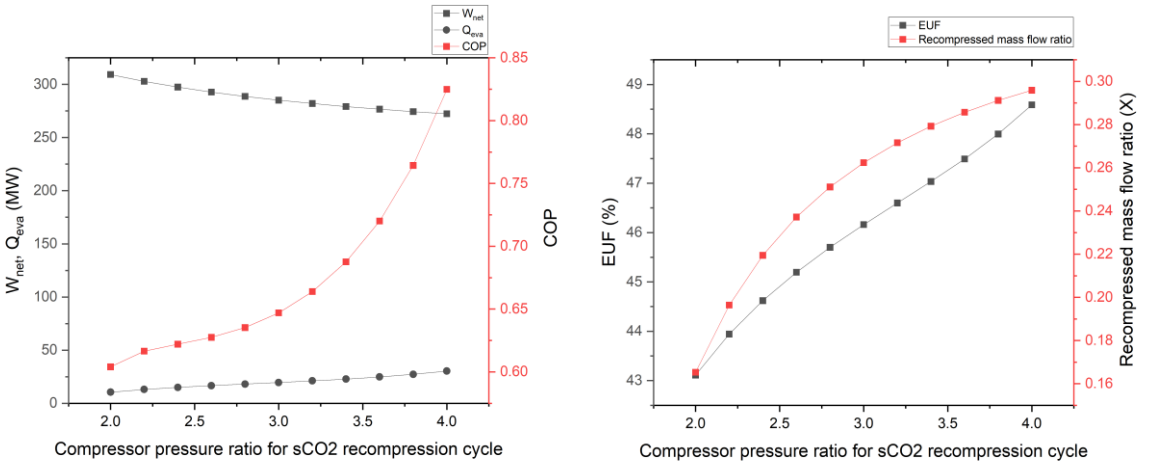

Fig. 3.13 Impact of pressure ratio of recompression cycle on overall performance parameters

the bottoming cycle's net power production is substantially lower than the top cycle's, the overall total power output is dictated by the sCO2 turbine's power delivery. When the pressure ratio of the cycle is increased, the decrease of enthalpy in the sCO2 turbine rises. This is why the power output of the sCO2 turbine grows at initially. When the impact of enthalpy increases does not compensate for the impact of a reduction in flow rate of mass, the sCO2 turbine power delivery declines. The integrated system's COP increases exponentially with the increase of PR.

A steep curve enhances the EUF as well as the recompression mass flow ratio. When tried to compare to the pump in the bottom cycle, the compressors' consumption power is dominant in the topping cycle. Thus, the entire cycle's net power output (W net) is mostly determined by the compressors' consumption power and the turbine's output. The delivered power of turbine and the used power of compressors both rise with a rise in PR with a unchanged inlet pressure (7.4 MPa) of the primary and recompression compressors. When the escalation of turbine's output work is

greater than that of the compressors, W_net of the entire cycle rises with PR; otherwise, W_net declines.

4.1.6 Effect of difference in temperature in the hot side of generator

The EUF falls while the recompression mass flow ratio remains unchanged,

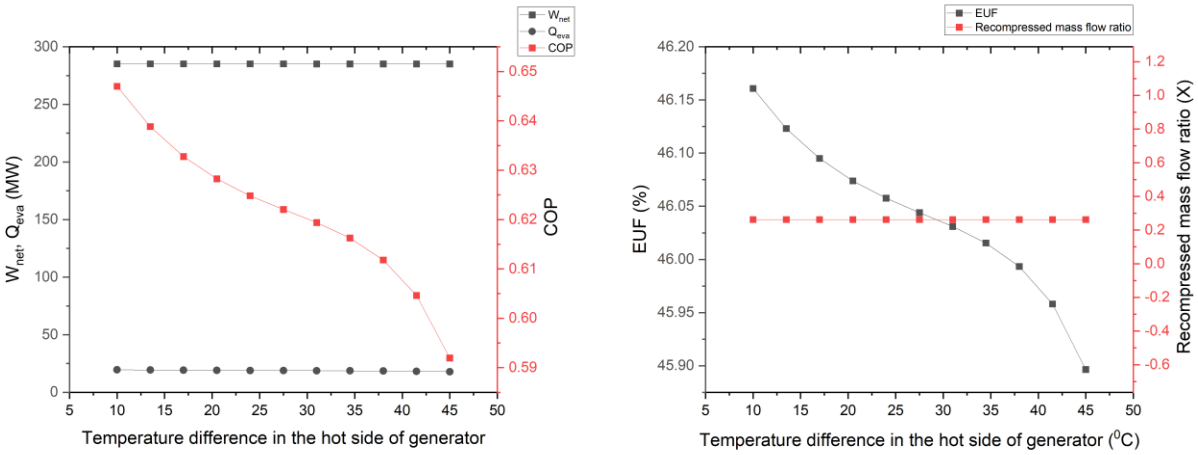

Fig. 3. 14 Effects of difference in temperature in the hot side of generator on overall performance parameters

as seen in Figure 3.14. The output temperature of LTR remains constant while temperature differential on hot side of the generator increases, and the heat flow in the generator gets greater, resulting in rising in heat (Q_ gen) consumed by ARC.

T_gen, on the other hand, diminishes as the temperature gradient between he hot as well as cold sides of generator increases. The COP drops as the temperature difference on the hot side of the generator increases, however Q_eva remains constant, implying that an acceptable temperature difference in the hot side of generator occurs for bottom ARC to achieve peak COP of Q_eva.

It was shown that when the temperature differential in the hot side of the generator increases, W_ net of combined cycle goes down slightly, owing to a little gain in W m in the ARC.

4.1.7 Impact of difference in temperature in the cold side of generator of ARC

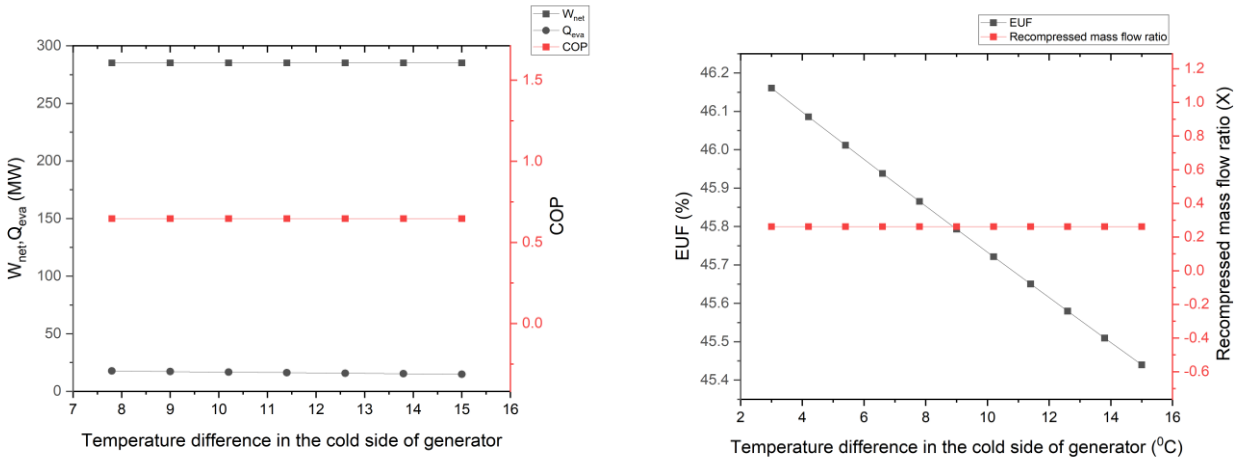

Fig. 3.15 Impacts of difference in temperature in the cold side of generator on overall performance

As can be displayed in Fig. 3.15, EUF decreased as the thermal gradient in the cold side of the generator increased, while the recompression mass flow ratio remained constant. When the temperature differential in the cold side of the generator fluctuates due to unchanged values of T_gen, T_cond, T_eva, and T_abs, the COP of an ARC remains constant. Q_eva diminishes as temperature differential between hot as well as cold sides of the generator grows.

Furthermore, as the temperature difference in cold side of the generator rises, W_net of the entire cycle shows a tiny rise, which is primarily due to a small drop in W_m of the bottom ARC. Furthermore, when thermal gradient in the cold side of the generator goes from 3 C to 15 C, the absolute increase in W_net is 0.014 MW, showing that W_ net is nearly constant. As shown in the previous analysis, the small increase in W_net is negligible to compensate for the increasing temperature gradient on the generator's cold

side.

4.1.8 Effect of evaporator temperature of ARC

It can be found in Fig. 3.16 that as T_eva rises, EUF rises as well. While the

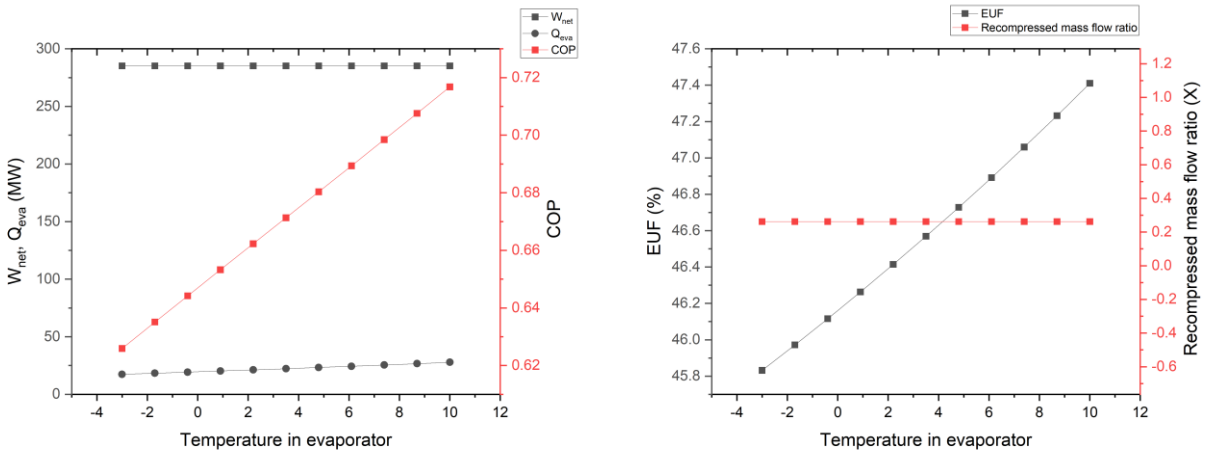

Fig. 3.16 Effect of evaporator temperature of ARC on overall performance parameters

other process variables remain constant, COP increases as T_eva grows for ammonia-water ARC. Meanwhile, as T_eva rises in current work, the generator can trap the heat (Q_gen). As a result, Q_eva rises in tandem with T_eva. Furthermore, because to lowering of W_m in the bottom ARC, W_net increases significantly as T eva increases.

When T_eva is increased from -2.9C up to 10C, the relative change in W_net is 0.012 MW, suggesting that W net remains nearly constant. As a result, the EUF's fluctuation trends are linked to Q_eva.

The overall net power production and overall heating capacity are unaffected by T_eva changes, however the refrigeration capacity increases. The cause for this is because when T_eva grows, the ejector's entrainment ratio rises, resulting in a increase in the secondary fluid's flow rate.

4.1.9 Effect of evaporator pressure of ORC

Due to the influence of ORC's evaporator pressure, the combined system's COP and Q_eva stay nearly unchanged. However, W_net has increased slightly, achieving a figure of roughly 300MW.

The EUF of the combined system rises dramatically as the evaporator pressure rises. The recompression mass flow ratio, on the other hand, stays unchanged at roughly 0.3.

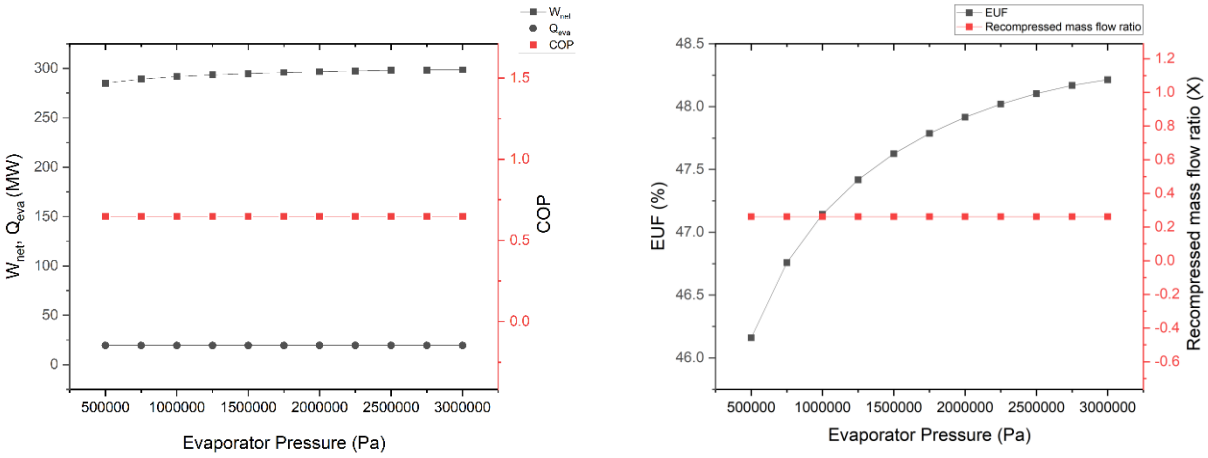

Fig. 3.17 Effect of evaporator pressure of ORC on overall performance parameters

Chapter 5

OUTLINES, FINDINGS AND SUGGESTIONS

5.1 Outlines

A new combined thermodynamic cycle was proposed, combining four cycles to use waste heat and make the system more efficient. A thermodynamic model was developed on the basis of energy balance equations of individual section of the cycles. The entire modeling process was carried out utilizing Python scripts and a variety of libraries. The parametric analysis of the cycles was carried out using an optimization approach. The effects of various decision factors on the energy usage factor (EUF), coefficient of performance (COP), net work done, and recompression mass flow ratio were graphically depicted.

5.2 Findings

Parametric analysis of the decision variables pressure ratio of gas turbine, inlet temperature of gas turbine, isentropic efficiencies of the air compressor, isentropic efficiencies of gas turbine, the pressure ratio of recompression cycle, the temperature difference in the hot side of generator of ARC, the difference in temperature of the cold side of the generator of ARC, evaporator temperature of ARC and evaporator pressure of ORC was done in comparison to W_net, Q_eva, COP, EUF, m.

With the exception of T gen hot, all of the parameters rise, resulting in an increase in W net. Except for T gen cold and T gen hot, EUF rises for all.

The increase in inlet temperature of gas turbine and pressure ratio of the recompression cycle affects COP of combined system, as does the decrease in gas turbine pressure ratio, isentropic efficiency of gas turbine, and the temperature difference in the hot side of ARC generator. EUF achieves a

high value of around 47%.

5.3 Suggestions

There are various other cycles that can be introduced and evaluated in addition to the ones included in the suggested model in this study. For higher system efficiency, the decision factors can be better adjusted through rigorous research. Instead of ammonia-water, there are a variety of fluids used in the system available in market that can be utilized in absorption refrigerating cycle. The proposed system's exergoeconomic analysis can be carried out. The heat for the whole system can be generated using a variety of power sources, as well as solar, nuclear, geothermal, and coal.

BIBLIOGRAPHY

[1] Y. Glavatskaya, P. Podevin, V. Lemort, O. Shonda, and G. Descombes, "Reciprocating Expander for an Exhaust Heat Recovery Rankine Cycle for a Passenger Car Application," *Energies* , vol. 5, no. 6. 2012, doi: 10.3390/en5061751.

[2] P. Roy, M. Désilets, N. Galanis, H. Nesreddine, and E. Cayer, "Thermodynamic analysis of a power cycle using a low-temperature source and a binary NH3–H2O mixture as working fluid," *Int. J. Therm. Sci.*, vol. 49, no. 1, pp. 48–58, Jan. 2010, doi: 10.1016/J.IJTHERMALSCI.2009.05.014.

[3] K. H. Kim, C. H. Han, and K. Kim, "Effects of ammonia concentration on the thermodynamic performances of ammonia–water based power cycles," *Thermochim. Acta*, vol. 530, pp. 7–16, Feb. 2012, doi: 10.1016/J.TCA.2011.11.028.

[4] U. Drescher and D. Brüggemann, "Fluid selection for the Organic Rankine Cycle (ORC) in biomass power and heat plants," *Appl. Therm. Eng.*, vol. 27, no. 1, pp. 223–228, Jan. 2007, doi: 10.1016/J.APPLTHERMALENG.2006.04.024.

[5] A. Pezzuolo, A. Benato, A. Stoppato, and A. Mirandola, "The ORC-PD: A versatile tool for fluid selection and Organic Rankine Cycle unit design," *Energy*, vol. 102, pp. 605–620, May 2016, doi: 10.1016/J.ENERGY.2016.02.128.

[6] R. V. Padilla, G. Demirkaya, D. Y. Goswami, E. Stefanakos, and M. M. Rahman, "Analysis of power and cooling cogeneration using ammonia-water mixture," *Energy*, vol. 35, no. 12, pp. 4649–4657, Dec. 2010, doi: 10.1016/J.ENERGY.2010.09.042.

[7] A. Fontalvo, H. Pinzon, J. Duarte, A. Bula, A. G. Quiroga, and R. V. Padilla, “Exergy analysis of a combined power and cooling cycle,” *Appl. Therm. Eng.*, vol. 60, no. 1–2, pp. 164–171, Oct. 2013, doi: 10.1016/J.APPLTHERMALENG.2013.06.034.

[8] M. Pouraghaie, K. Atashkari, S. M. Besarati, and N. Nariman-zadeh, “Thermodynamic performance optimization of a combined power/cooling cycle,” *Energy Convers. Manag.*, vol. 51, no. 1, pp. 204–211, Jan. 2010, doi: 10.1016/J.ENCONMAN.2009.09.014.

[9] A. Habibzadeh, M. M. Rashidi, and N. Galanis, “Analysis of a combined power and ejector-refrigeration cycle using low temperature heat,” *Energy Convers. Manag.*, vol. 65, pp. 381–391, 2013, doi: 10.1016/j.enconman.2012.08.020.

[10] E. Galloni, G. Fontana, and S. Staccone, “Design and experimental analysis of a mini ORC (organic Rankine cycle) power plant based on R245fa working fluid,” *Energy*, vol. 90, pp. 768–775, Oct. 2015, doi: 10.1016/J.ENERGY.2015.07.104.

[11] S. Shaaban, “Analysis of an integrated solar combined cycle with steam and organic Rankine cycles as bottoming cycles,” *Energy Convers. Manag.*, vol. 126, pp. 1003–1012, Oct. 2016, doi: 10.1016/J.ENCONMAN.2016.08.075.

[12] A. Kouta, F. A. Al-sulaiman, and M. Atif, “Energy analysis of a solar driven cogeneration system using supercritical CO 2 power cycle and MEE-TVC desalination system,” *Energy*, 2016, doi: 10.1016/j.energy.2016.11.041.

[13] X. Shi and D. Che, “A combined power cycle utilizing low-temperature waste heat and LNG cold energy,” *Energy Convers. Manag.*, vol. 50, no. 3, pp. 567–575, Mar. 2009, doi:

10.1016/J.ENCONMAN.2008.10.015.

[14] A. Vidal, R. Best, R. Rivero, and J. Cervantes, “Analysis of a combined power and refrigeration cycle by the exergy method,” *Energy*, vol. 31, no. 15, pp. 3401–3414, Dec. 2006, doi: 10.1016/J.ENERGY.2006.03.001.

[15] Y. M. El-Sayed and M. Tribus, “A theoretical comparison of the Rankine and Kalina cycles,” *ASME Publ. AES*, vol. 1, pp. 97–102, 1985.

[16] H. D. Madhawa Hettiarachchi, M. Golubovic, W. M. Worek, and Y. Ikegami, “The Performance of the Kalina Cycle System 11(KCS-11) With Low-Temperature Heat Sources,” *J. Energy Resour. Technol.*, vol. 129, no. 3, pp. 243–247, Feb. 2007, doi: 10.1115/1.2748815.

[17] H. Jouhara, N. Khordehgah, S. Almahmoud, B. Delpech, A. Chauhan, and S. A. Tassou, “Waste heat recovery technologies and applications,” *Therm. Sci. Eng. Prog.*, vol. 6, pp. 268–289, Jun. 2018, doi: 10.1016/J.TSEP.2018.04.017.

[18] R. Loni, G. Najafi, E. Bellos, F. Rajaee, Z. Said, and M. Mazlan, “A review of industrial waste heat recovery system for power generation with Organic Rankine Cycle: Recent challenges and future outlook,” *J. Clean. Prod.*, vol. 287, p. 125070, Mar. 2021, doi: 10.1016/J.JCLEPRO.2020.125070.

[19] Z. Y. Xu, R. Z. Wang, and C. Yang, “Perspectives for low-temperature waste heat recovery,” *Energy*, vol. 176, pp. 1037–1043, Jun. 2019, doi: 10.1016/J.ENERGY.2019.04.001.

[20] R. Chacartegui, D. Sánchez, J. M. Muñoz, and T. Sánchez, “Alternative ORC bottoming cycles FOR combined cycle power

plants," *Appl. Energy*, vol. 86, no. 10, pp. 2162–2170, Oct. 2009, doi: 10.1016/J.APENERGY.2009.02.016.

[21] G. Fan, H. Li, Y. Du, S. Zheng, K. Chen, and Y. Dai, "Preliminary conceptual design and thermo-economic analysis of a combined cooling , heating and power system based on supercritical carbon dioxide cycle," *Energy*, vol. 203, p. 117842, 2020, doi: 10.1016/j.energy.2020.117842.

[22] A. De Pascale, C. Ferrari, F. Melino, M. Morini, and M. Pinelli, "Integration between a thermophotovoltaic generator and an Organic Rankine Cycle," *Appl. Energy*, vol. 97, pp. 695–703, Sep. 2012, doi: 10.1016/J.APENERGY.2011.12.043.

[23] F. Petrakopoulou, G. Tsatsaronis, T. Morosuk, and A. Carassai, "Conventional and advanced exergetic analyses applied to a combined cycle power plant," *Energy*, vol. 41, no. 1, pp. 146–152, May 2012, doi: 10.1016/J.ENERGY.2011.05.028.

[24] A. M. Bassily, "Modeling, analysis, and modifications of different GT cooling techniques for modern commercial combined cycle power plants with reducing the irreversibility of the HRSG," *Appl. Therm. Eng.*, vol. 53, no. 1, pp. 131–146, Apr. 2013, doi: 10.1016/J.APPLTHERMALENG.2013.01.002.

[25] A. G. Kaviri, M. N. M. Jaafar, T. M. Lazim, and H. Barzegaravval, "Exergoenvironmental optimization of Heat Recovery Steam Generators in combined cycle power plant through energy and exergy analysis," *Energy Convers. Manag.*, vol. 67, pp. 27–33, Mar. 2013, doi: 10.1016/J.ENCONMAN.2012.10.017.

[26] N. Modi, B. Pandya, and J. Patel, "Comparative analysis of a solar-driven novel salt-based absorption chiller with the

implementation of nanoparticles," *Int. J. Energy Res.*, vol. 43, no. 4, pp. 1563–1577, 2019.

[27] Y. Bicer and I. Dincer, "Analysis and performance evaluation of a renewable energy based multigeneration system," *Energy*, vol. 94, pp. 623–632, Jan. 2016, doi: 10.1016/J.ENERGY.2015.10.142.

[28] Y. Ahn *et al.*, "Review of supercritical CO2 power cycle technology and current status of research and development," *Nucl. Eng. Technol.*, vol. 47, no. 6, pp. 647–661, Oct. 2015, doi: 10.1016/J.NET.2015.06.009.

[29] V. Dostal, M. J. Driscoll, P. Hejzlar, and N. E. Todreas, "A Supercritical CO2 Gas Turbine Power Cycle for Next-Generation Nuclear Reactors." pp. 567–574, Apr. 2002, doi: 10.1115/ICONE10-22192.

[30] R. V. Padilla, Y. C. Soo Too, R. Benito, and W. Stein, "Exergetic analysis of supercritical CO2 Brayton cycles integrated with solar central receivers," *Appl. Energy*, vol. 148, pp. 348–365, Jun. 2015, doi: 10.1016/J.APENERGY.2015.03.090.

[31] U. B. Kaupp and R. Seifert, "Cyclic nucleotide-gated ion channels," *Physiol. Rev.*, vol. 82, no. 3, pp. 769–824, 2002.

[32] P. E. Savage, S. Gopalan, T. I. Mizan, C. J. Martino, and E. E. Brock, "Reactions at supercritical conditions: Applications and fundamentals," *AIChE J.*, vol. 41, no. 7, pp. 1723–1778, 1995, doi: 10.1002/aic.690410712.

[33] P. Nikolai, B. Rabiyat, A. Aslan, and A. Ilmutdin, *Supercritical CO 2 : Properties and Technological Applications - A Review*, no. July. 2019.

[34] G. Sulzer, "Verfahren zur erzeugung von arbeit aus warme (Method for

producing work from heat),” *Swiss Pat.*, vol. 269599, 1948.

[35] D. P. Gokhshtein and G. P. Verkhivker, “Use of carbon dioxide as a heat carrier and working substance in atomic power stations,” *Sov. At. Energy*, vol. 26, no. 4, pp. 430–432, 1969.

[36] G. Angelino, “Carbon dioxide condensation cycles for power production,” 1968.

[37] J. R. Hoffmann and E. G. Feher, “150 kwe Supercritical Closed Cycle System,” *J. Eng. Power*, vol. 93, no. 1, pp. 70–80, Jan. 1971, doi: 10.1115/1.3445409.

[38] A. Valero *et al.*, “CGAM problem: Definition and conventional solution,” *Energy*, vol. 19, no. 3, pp. 279–286, 1994, doi: https://doi.org/10.1016/0360-5442(94)90112-0.

[39] V. Dostal, M. J. Driscoll, and P. Hejzlar, “A Supercritical Carbon Dioxide Cycle for Next Generation Nuclear Reactors,” MIT, 2004.

[40] C. S. Turchi, Z. Ma, T. W. Neises, and M. J. Wagner, “Thermodynamic study of advanced supercritical carbon dioxide power cycles for concentrating solar power systems,” *J. Sol. Energy Eng. Trans. ASME*, vol. 135, no. 4, pp. 1–7, 2013, doi: 10.1115/1.4024030.

[41] M. Kulhánek and V. Dostál, “Thermodynamic Analysis and Comparison of Supercritical Carbon Dioxide Cycles.”

[42] D.-W. Sun, “Comparison of the performances of NH3-H2O, NH3-LiNO3 and NH3-NaSCN absorption refrigeration systems,” *Energy Convers. Manag.*, vol. 39, no. 5, pp. 357–368, 1998, doi: https://doi.org/10.1016/S0196-8904(97)00027-7.

[43] Y. Liu, Y. Wang, and D. Huang, “Supercritical CO2 Brayton cycle: A state-of-the-art review,” *Energy*, vol. 189, p. 115900, 2019, doi: https://doi.org/10.1016/j.energy.2019.115900.

[44] M. Mehrpooya, M. M. M. Sharifzadeh, and M. H. Katooli, “Thermodynamic analysis of integrated LNG regasification process configurations,” *Prog. Energy Combust. Sci.*, vol. 69, pp. 1–27, 2018, doi: https://doi.org/10.1016/j.pecs.2018.06.001.

[45] J. Song, X. Li, X. Ren, and C. Gu, “Performance analysis and parametric optimization of supercritical carbon dioxide (S-CO2) cycle with bottoming Organic Rankine Cycle (ORC),” *Energy*, vol. 143, pp. 406–416, 2018, doi: https://doi.org/10.1016/j.energy.2017.10.136.

[46] C. Wu, S. Wang, X. Feng, and J. Li, “Energy, exergy and exergoeconomic analyses of a combined supercritical CO2 recompression Brayton/absorption refrigeration cycle,” *Energy Convers. Manag.*, vol. 148, pp. 360–377, 2017, doi: https://doi.org/10.1016/j.enconman.2017.05.042.

[47] M. Yari and S. M. S. Mahmoudi, “A thermodynamic study of waste heat recovery from GT-MHR using organic Rankine cycles,” *Heat Mass Transf. und Stoffuebertragung*, vol. 47, no. 2, pp. 181–196, 2011, doi: 10.1007/s00231-010-0698-z.

[48] M. Khaljani, R. Khoshbakhti Saray, and K. Bahlouli, “Comprehensive analysis of energy, exergy and exergo-economic of cogeneration of heat and power in a combined gas turbine and organic Rankine cycle,” *Energy Convers. Manag.*, vol. 97, pp. 154–165, 2015, doi: 10.1016/j.enconman.2015.02.067.

[49] S. Hou, Y. Zhou, L. Yu, F. Zhang, and S. Cao, “Optimization of the combined supercritical CO2 cycle and organic Rankine cycle using

zeotropic mixtures for gas turbine waste heat recovery," *Energy Convers. Manag.*, vol. 160, no. January, pp. 313–325, 2018, doi: 10.1016/j.enconman.2018.01.051.

CERTIFICATE OF RESEARCH

This thesis titled "Thermodynamic Investigation of Combined Cycles And Polygeneration Systems With An Emphasis On Supercritical Carbon Dioxide Power Cycles" submitted by SALIM SADMAN BISHAL (170011014) and DEWAN FAHIM FAYSAL (170011036) has been accepted as satisfactory in partial fulfillment of the requirement for the Degree of Bachelor of Science in Mechanical Engineering.

Supervisor

10.06.2022

Dr. Mohammad Monjurul Ehsan
Associate Professor
Department of Mechanical and Production Engineering (MPE)
Islamic University of Technology (IUT)

Head of the Department

10/06/2022

Dr. Md. Anayet Ullah Patwari
Professor
Department of Mechanical and Production Engineering (MPE)
Islamic University of Technology (IUT)

DECLARATION

We hereby declare that this thesis entitled "Thermodynamic Investigation of Combined Cycles And Polygeneration Systems With An Emphasis On Supercritical Carbon Dioxide Power Cycles" is an authentic report of our study carried out as requirement for the award of degree B.Sc. (Mechanical Engineering) at Islamic University of Technology, Gazipur, Dhaka, under the supervision of Dr. Mohammad Monjurul Ehsan, Associate Professor, MPE, IUT in the year 2022

The matter embodied in this thesis has not been submitted in part or full to any other institute for award of any degree.

Salim Sadman Bishal

Salim Sadman Bishal
170011014

Dewan Fahim

Dewan Fahim Faysal
170011036